NUST COLLEGE OF
ELECTRICAL AND MECHANICAL ENGINEERING

DESIGN AND FABRICATION OF EXPERIMENTAL SETUP TO STUDY THE EROSION OF STEEL BY WET SAND PARTICLE IMPACT

A PROJECT REPORT

DE-40(DME)

THE YEAR 2022

Submitted by:

MUHAMMAD ALI FAHAD

UMAR SHERAZ

MUHAMMAD MOIN UD DIN

MUHAMMAD ABDULLAH

PROJECT SUPERVISOR

DR. MUHAMMAD REHAN KHAN

NUST COLLEGE OF ELECTRICAL AND MECHANICAL ENGINEERING

DECLARATION

We thus certify that no aspect of the work described in this project report has been used to assist an application for another degree or qualification at any other university or institute of education. If we are proven guilty of plagiarism, we shall be liable for any legal action taken against us, which might include the revocation of our degree, based on the intensity of the offense.

COPYRIGHT STATEMENT

ACKNOWLEDGEMENTS

We are grateful to Allah Almighty, the Most Merciful, and Al Fattah for bestowing upon us His blessings, courage, and wisdom, which have enabled us to attain such a beautiful goal.

In the face of adversity, we are grateful to our parents and family for their unfailing support and encouragement. We owe our supervisor, Dr. Muhammad Rehan Khan, a debt of appreciation for his continual guidance and time spent supporting and encouraging us at each stage. Without his efforts, we would not have been able to accomplish so much. We are also grateful to all of our colleagues and friends who aided us both intellectually and emotionally. Many thanks to everyone who helped; things may have turned out differently if it hadn't been for everyone's support and admiration. We hope that this effort will add value to people's lives and that it will be expanded further so that this may be widely used.

ABSTRACT

Slurry erosion is responsible for major failures in oil and gas transmission pipelines. During petroleum production, sand particles can be entrained with the transported carrier fluid despite any sand exclusion process and erode the inner walls of the pipelines. This erosion process may even cause pipe leakage and oil spill. Therefore, investigating the regularities of erosion damage changing with particle size and predicting erosion behavior for different particle sizes are important to pipeline safety. In this study, the slurry erosion behavior of AISI 1018 carbon steel is investigated to determine the effect of three different parameters on the erosion rate of the targeted material. These parameters are flow velocity, impingement angle, and erodent particle size. We investigated the erosion of steel caused by wet sand particles. Carbon steel will be used as it is the most deployed material in the industry. There are two options either to use an elbow shape plate or a flat plate. We opted for a flat plate of carbon steel as all erosion models had been developed for flat plates. There are two ways to study the erosion of materials. The first is the flow loop and the second is the direct impact test. We applied a direct impact test as in this test we can control the flow and impact conditions. Fine sand was of concern for us in terms of erosion as its size is almost 62.5microns which is less than the size of sieve mesh whose size is 75 microns. The very first step of the whole procedure was polishing. Flat plates can be polished easily as compared to elbow shape plates. The confocal microscope is not available, so we used the digital microscope. The direct mass loss was measured to quantify the erosion rate of the test specimens. Qualitative techniques such as multilayer paint modeling and microscopic surface imaging are also used to scrutinize the flow accelerated erosion mechanism.

TABLE OF CONTENTS

LIST OF FIGURES

LIST OF TABLES

CHAPTER 1

INTRODUCTION

1.1 Background

The surface degradation of the equipment caused by repeated collisions of abrasive particles transported by the fluid is called solid particle erosion[1]. Pipelines are the most cost-effective and versatile method of transporting oil and gas from production sites to end users, and they may survive for decades with little maintenance. In the oil and gas sector, low carbon steels and high strength low alloy steels (HSLA) pipes are widely utilized. Erosion has become a problem as the working pressure of pipelines has been increased to fulfill the ever-increasing demand for energy. Three phases, a carrier liquid (oil), hard solid particles (erodent particles), and the material surface, coexist. It is responsible for slurry erosion in pipelines[2]. The pipe wall thickness is reduced by this complicated mode of failure[3]. Pipes have a shorter lifespan because of this. This might result in irreparable harm to society and the environment. Erosion by sand particles is the most typical technique of material removal. It is a major concern in the oil and gas sector[4].

The hydrocarbon and mineral processing sectors are particularly prone to this. Sand particles as well as other imperfections unavoidably pollute hydrocarbon fluids collected from reservoirs. It is recognized as one of the most difficult hydrocarbons extraction related challenges. The process of obtaining crude oil from a reservoir entails complicated operations that, if not managed appropriately, can result in major economic damage and/or mortality. Due to the poorly consolidated nature of the extraction process, sand is produced alongside other fluids such as water, oil, and gas. Sanding during oil and gas production is directly responsible for many of the operational issues that the oil and gas industry faces[5, 6]. The carrier fluid transports these sand particles, causing damage to the pipeline's internal surface. It also causes equipment to fail, and the entire process's operational safety is jeopardized. As a result, slurry erosion has gotten a lot of attention from scholars in recent years[7-16].

Many efforts have been made to gain a fundamental knowledge of this complicated failure mode by proposing models and processes that account for experimental erosion rates under various operating settings[17-21]. However, investigating a single variable is difficult since all these components are interconnected[12]. As a result, researchers have endeavored to establish a link between erosion rate and influencing variables[22].

The influence of these parameters on the slurry erosion behavior of materials has been the subject of much investigation[23, 24]. Erosion is caused by a variety of destructive processes and a series of mechanical events[25]. Many sanding-related mishaps have been documented in the past, with leakage incidents occurring as a result of flow-line erosion. Figure 1.1 represents some of these incidents.

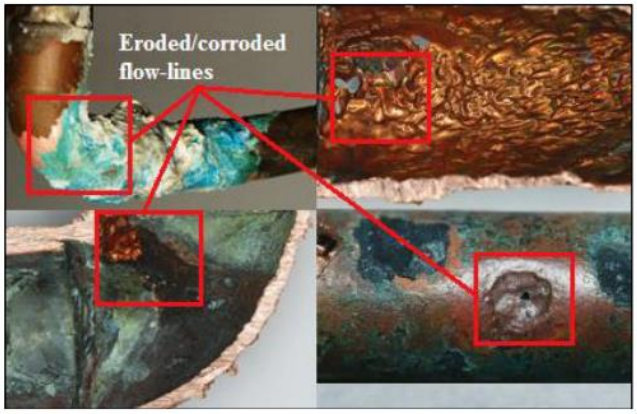

Figure 1. 1 A representation of spoiled flowlines caused by erosion-corrosion[26]

According to a data analysis of 432 oil pipeline failures from 2010 to 2015, erosion/corrosion is the major cause of these incidents, as illustrated in figure 1.2.

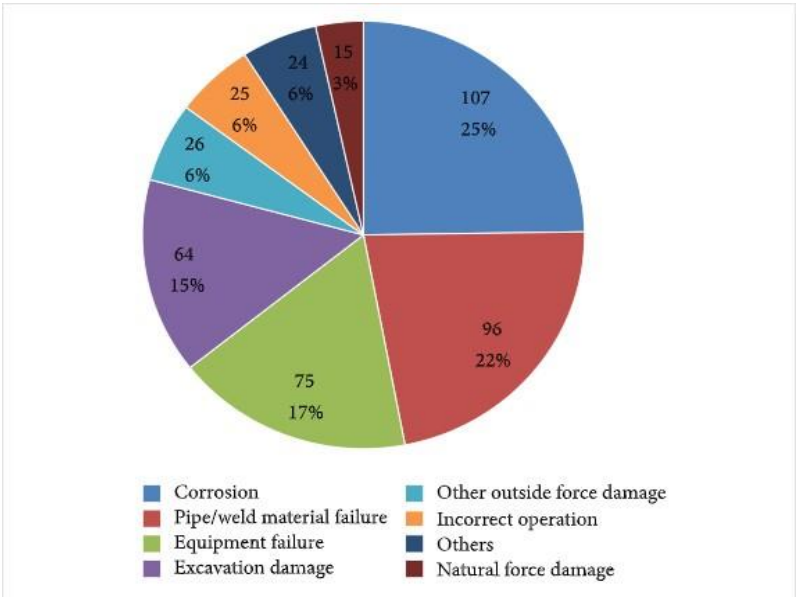

Figure 1. 2 Oil pipeline failure data from 2010 to 2015[27]

Although liquid droplet interactions and cavitation can cause erosion, it is widely acknowledged that solid particle erosion is the most prevalent form of erosion in the petroleum sector. Particularly, erosion due to fine sand particles is a serious concern in the hydrocarbon extraction and mineral processing industries. Fines are sand particles with a diameter of less than 62 microns that pass through a No. 200 (0.075 mm) sieve[28].

As a result of these particles, pipelines are degrading. Additionally, these are detrimental to the manufacturing process, operational safety, and flow efficiency. Sand filters or gravel packs are used at the entry of important manufacturing lines to solve this problem. But these ordinary sand screens are unable to prevent small particles (less than 62.5 microns) from becoming entrained in the fluid phase. As a result, these particles degrade pipes as they pass through sand filters.

Elbows, tees, pumps, valves, chokes, and other piping fittings are used in the oil and gas industry to transfer fluids. It is noteworthy that areas where the flow direction abruptly changes during the manufacturing and transportation process are the most susceptible to particle erosion. Flow direction alters within these geometries, as sand particles cross streamlines and approach internal walls. It happens because of inertia and turbulent dispersion. These particles inflict harm to the interior walls when they travel at high speeds. The pipe wall deteriorates because of repeated high-speed collisions with many particles. Erosion damage causes leaks and sudden failures of downhole tubes, subsea hardware, and pipelines in the oil and gas sector, resulting in costly repairs and lost production time. As a result, it is critical to forecast the rate of erosion and pinpoint the most vulnerable equipment.

Predicting the degree of erosion in oilfield equipment is critical for ensuring equipment reliability and avoiding production issues. Furthermore, high-precision erosion projection aids in the design of equipment with minimal erosion effects during service. Many studies have already been carried out to create empirical and numerical models for sand impact erosion forecasts. Numerous parameters have been discovered that affect the erosion process, all of which should be considered while constructing an erosion model. Sand particle impact speed, angle, particle characteristics (size, sharpness, hardness), and target material hardness are all the most important factors that influence erosion rate. Erosion estimation techniques that are either mechanistic or based on Computational Fluid Dynamics (CFD) were created with these crucial elements in mind.

Particle concentration determines the rate of erosion to a large extent. The investigation of the erosion mechanism is complicated by a lack of understanding of particle concentration and its impact on the erosion mechanism. A better understanding of particle concentration is essential for comprehending the multiphase erosion process. Most of the available erosion data come from direct impact tests. The precision of the direct impact

test, on the other hand, is limited to single-phase flow conditions and flat target surfaces. As a result, experiments to obtain quantitative and qualitative erosion-induced damage results for multiphase flow conditions are required to address the complexities of a multiphase erosion problem and to quantify erosion distribution and rate for working conditions that are more like field operating conditions.

1.2 Problem Statement

Erosion-induced damage in the pipe system increases as sand particles pass through sand filters. It causes equipment failure which needs to be replaced then. A better comprehension of the erosion mechanism leads to improved pipeline operating conditions. Despite all the previous research on a variety of parameters that may influence erosion, there are still some that have not been well explored. For example, erosion from sand fines has not received nearly as much attention as erosion from big particles. More research is needed to successfully anticipate sand fines erosion. The presence of these sand particles is hypothesized to hasten material degradation by generating inhomogeneous pits to form at various locations around the pipelines due to particle impaction, rebound, and mass transfer. Carbon steel erosion has been identified as a major problem in the hydrocarbon and mineral processing sectors. As a result, the primary goal of this research is to provide a mechanistic understanding and correlation of erosion caused by sand particles in multiphase flow and to accomplish effective erosion control.

1.3 Motivation for the proposed research

The motivation behind this research was to fill the knowledge gap and to fulfill the technological needs by experimentally evaluating the erosion mechanism in multiphase flow conditions based on flow loop experimentation. Previous research indicated that there was little research on erosion mechanisms due to fine sand as compared to that due to larger particles. This was our research gap, and we tried our best to fulfill this gap by doing this research.

1.4 Objectives

This research was aimed to develop and improve the understanding of the degradation behavior of carbon steel flat plates in a multiphase (water-sand) flow conditions under erosion circumstances through the following objectives:

- To investigate the degradation behavior of carbon steel flat plate in multiphase (water-sand) flow conditions.

- To quantify the erosion rate by considering three important parameters. (a) flow velocity (b) Particle size (c) Impact angle

1.5 Scope of Study

This study aims to quantify the degradation rate of low carbon 1018 steel flat plates by varying different parameters like impact angle, flow velocity, and particle size. Sand particles of 50 microns and 60 microns were utilized in testing. Experiments were performed at three different velocities 4 m/s, 6 m/s, and 8 m/s. Impingement angles of 30 degrees, 60 degrees, and 90 degrees were employed during testing.

1.6 Outline of the Thesis

There are five chapters in this paper. The Introduction, objectives, and scope of the study are discussed in Chapter 1. Furthermore, a literature review and different erosion models with equations are included in Chapter 2. In Chapter 3, methodology, material characterization, and parameter selection are explained. Moreover, the methods, initial design, challenges we had to encounter in our project, and how we overcome those challenges and carried out our project are also discussed briefly. In chapter 4 we have presented our results and findings and performed certain comparisons to distinguish between different parameters and how those parameters were related to each other. In chapter 5, we have given the conclusion of our research and future recommendations for the improvement in this field of study.

CHAPTER 2

LITERATURE REVIEW

2.1 Introduction

This chapter gives a review of the previous research on the erosion mechanism and its prediction. This provides more insight understanding and realizing the potential of the present work. Section 2.2 of this chapter covers erosion mechanisms. Ductile and brittle materials are not eroded via the same mechanism. Erosion mechanisms are different for both ductile and brittle materials. Section 2.3 is about parameters that mainly influence erosion rate. Effect of impact velocity, impingement angle, erodent properties (size, hardness, and shape), erodent concentration, erodent viscosity, and characteristics of targeted material on erosion rate is described in this section. Section 2.4 explains different types of erosion tests. Each test is used to determine the erosion rate but by applying different techniques. Section 2.5 deals with the modeling of the solid particle erosion mechanism. These models include mechanistic erosion models, theoretical erosion equations, and empirical erosion equations. Section 2.6 summarizes this chapter.

2.2 Sand Particle Erosion Mechanism

Erosion is an intricate phenomenon in which multiple mechanisms operate at the same time that depends on each other. The effect of these multiple mechanisms at the same time determines the overall erosion rate. Scanning electron microscopy (SEM) examinations of the degraded surfaces give the results of this area. Literature shows that erosion mechanisms in ductile and brittle materials are not same. The following sections discuss erosion mechanisms in both types of material.

2.2.1 Erosion Mechanism in Ductile Material

Plastic deformation is a major process in the erosion of ductile material. Finnie [29] was the first person who created an erosion model of ductile materials in 1958. He argued that material degradation is a micro-machining mechanism, in the case of ductile material. His research was proved to be accurate as results were very close to experimental data but only at low impact angles. At high impact angles, results were not matching with experimental findings. He predicted almost no erosion at 90 degrees. According to his research, a crater is formed when erodent hit the surface at a low impingement angle. After making a crater, these particles leave the surface. The upcoming particles eliminate the fragment that was built by earlier collision, as shown in figure 2.1. It was felt that

another mechanism was required to demonstrate the erosion mechanism. Bitter [8] in 1963 proposed an erosion model afterward. He found out that cutting wear and deformation were two separate mechanisms that contributed to the erosion mechanism. The erosion damage that occurs at high impact angles may be explained by the plastic deformation outlined in Bitter's model. In 1986, another researcher came up with his idea. He was Levy [30] who proposed a platelet mechanism. He considered this mechanism a primary constituent of the erosion process in ductile materials. According to his work, a platelet is formed when metal is extruded due to a collision between particle and surface. At this point, there is no material loss. The tiny platelet is then forged and strewn throughout the surface.

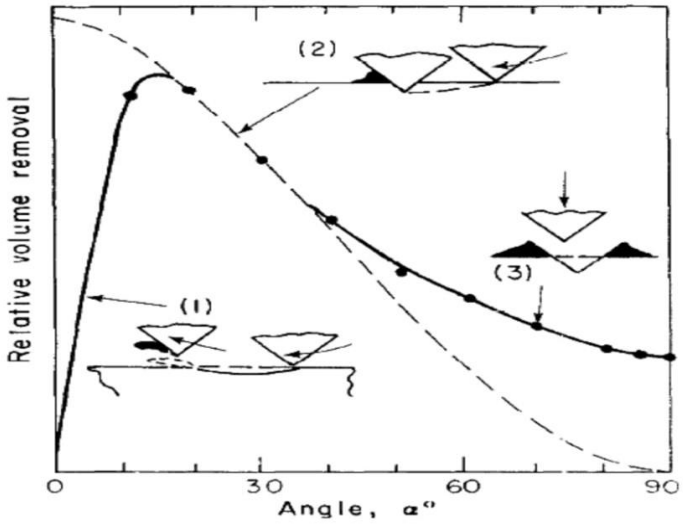

Figure 2. 1 Predicted variation in volume reduction with Angle (Curves 1, 2) and normalization of experimental values with maximum erosion (curve 3)

Moreover, platelet production and adiabatic shear heating occur simultaneously. Work hardened zone is also formed due to the high kinetic energy of erodent particles. At the beginning of the erosion exposure, a work-hardened zone form. The formation of platelets, craters, and work-hardened zone initiates the steady-state erosion mechanism. According to Levy [30], the initial erosion rate is always less than the steady-state erosion rate.

When platelets and craters have generated all over the designated surface and the work-hardened zone has achieved its full thickness and hardness, steady-state degradation commences. As a result, the steady-state erosion rate is greater than the initial erosion rate [30]. Hutchings and Winter [31] in 1974 proposed another model. They hit the steel balls of 3mm diameter at a tilted surface. They employed Scanning electron microscopy

(SEM) to investigate the degraded surface. They claimed that the formation of the lip at the crater's end was responsible for the removal of material. Shearing or extrusion of the metal surface resulted in lip generation. In the creation of the lip, the frictional force is crucial. Furthermore, the investigations revealed that when impact velocities were above a certain threshold, the lip would break from its base.

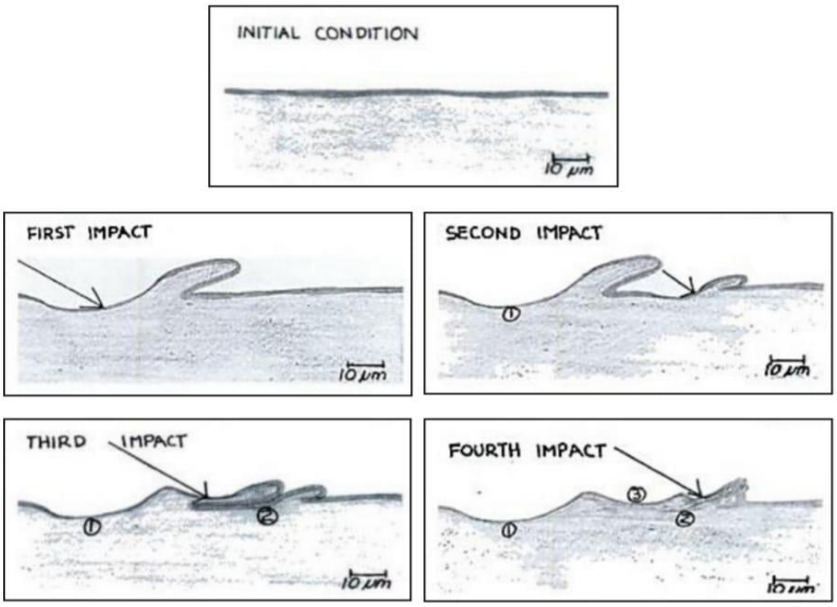

Figure 2. 2 Proposed Copper-Plated Steel Erosion Sequence [30]

Tilly [32] in 1973 proposed that the erosion mechanism in ductile materials consists of two stages. During the first stage, an indentation is created due to the collision of abrasive particles with the surface, which may result in the removal of the chip from that surface. During the second stage, particles break down into smaller fragments that project radially from the initial position. This breaks down of particles results in secondary damage. The particle breaks apart in the second step, and pieces are projected radially from the initial location. Secondary damage may occur because of fragmentation. A significant number of different investigations have been undertaken to uncover the erosion mechanism of ductile materials due to the intricacy of the erosion process. However, it is beyond the scope of this paper to go into detail about the other past works in this field.

2.2.2 Erosion Mechanism in Brittle Material

According to Levy [33], the creation and propagation of cracks are the primary reasons for brittle material degradation. Cone cracks arise due to the impingement of round particles on the surface. These cracks propagate inward. The middle and lateral cracks

appear as the contact stress rises. When the material is unloaded after the abrasive particle rebounds, the lateral cracks will advance until they contact each other and tear apart the interface area. This results in the elimination of material and the formation of a hemispheric crater. Figure 2.3 shows how brittle materials generate and expand cone, median, and lateral fractures, resulting in a hemispheric eroded crater.

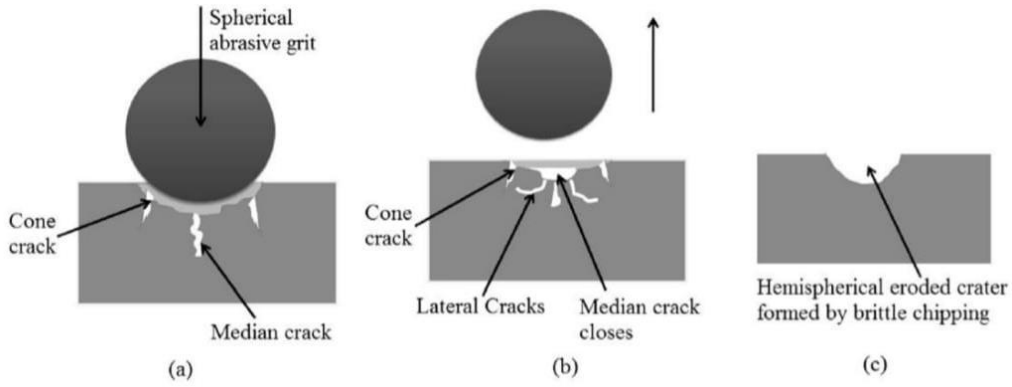

Figure 2. 3 Solid particle erosion mechanism in material

2.3 Influencing Parameters in Solid Particle Erosion

Many factors influence the solid particle erosion mechanism. Identification of these crucial parameters is important to comprehend this erosion phenomenon and to build accurate erosion models. Meng and Ludema [34] in 1995 identified 33 important parameters that play important role in the material degradation process. Most of these parameters are not independent and are linked with other factors. Clark [35] and Javaheri et al [36] in 2002 also pointed out some crucial parameters that affect the erosion mechanism in slurry flow. Figure 2.1 represents these important factors that are identified by Clark [35] and Javaheri et al [36]. The following sections explain some of these important parameters.

2.3.1 Particle Impact Velocity

Finnie [29] in 1960 developed a theoretical equation to estimate the erosion rate. According to his studies, erodent impact velocity directly influences erosion rate and erosion mechanism. Equation 2.1 illustrates the relationship between erosion rate and impact velocity of the particle as follows.

$$ER \propto V_p^n \tag{2.1}$$

Here, ER represents the erosion rate and Vp denotes particle impact velocity. Finnie discovered in the early phases of his research that the erosion rate (ER) is related to the square of the impact velocity (Vp). Further experiments revealed that the impact velocity exponent (n) was more than 2.0. (Usually about 2.3 or 2.4). After these experimental tests, Finnie in 1995 found out the reason behind this increase in the exponent. He said that the rotation of particles was accountable for this increase in velocity exponent. This rotation was not taken into consideration in the previous formulation. As a result of it, an additional term was introduced that was dependent on the cubic exponent of velocity. A single term can be approximated with an exponent of velocity greater than 2. According to Tilly [32], an erosion mechanism can be divided into two different stages. The primary damage occurs during the first stage owing to initial particle collision, which leads to the creation of an indentation and the elimination of a metal chip. Particles split up and pieces hit the targeted material during the second step. Because of the particle segmentation, the impact velocity exponent is more than 2. For 90-degree strikes, Laitone [37] discovered in 1979 that the erosion in ductile materials varies with the fourth power of impact velocity. While at shallow angles, the velocity exponent was greater than 2 but less than 4. Oka et al. [38] in 2005 came with the results exponent of particle impact velocity is dependent upon material hardness and particle shape. Therefore, he included the hardness factors in his model. He also revealed that particle impact velocity does not depend on the diameter of the particle.

2.3.2 Particle Impact Angle

Previous research has shown that the angle of impact of a particle influences the rate of degradation. The link between wear rate and impact angle is mostly determined by material hardness. As a result, in ductile and brittle materials, this correlation does not hold true. The relationship between erosion rate and particle impingement angle is determined by the qualities of the eroded material, specifically the material hardness. As a result, ductile and stiff materials have different erosion rates as a function of impact angle. Hutching [39] investigated the effect of impact angle on erosion rate for brittle and ductile solids in 1992. His findings are depicted in Figure 2.4. At lower angles of incidence (between 15 and 40 degrees), the wear rate in ductile material rapidly rises to a maximum value, then progressively drops. The most common modes in ductile materials are cutting and ploughing, which typically happen at low impact angles. As a result, ductile materials' maximum erosion value is found at a lower impingement angle.

The highest erosion rate occurs in brittle materials when particles impact the surface at a 90-degree angle frequently). Permanent deformation at a higher impingement angle causes this erosion damage. In erosion studies, Oka et al. [38] discovered that the particle impact angle is unaffected by particle velocity or size. The hardness of the material and the kind of sand particles have no bearing on the impact angle.

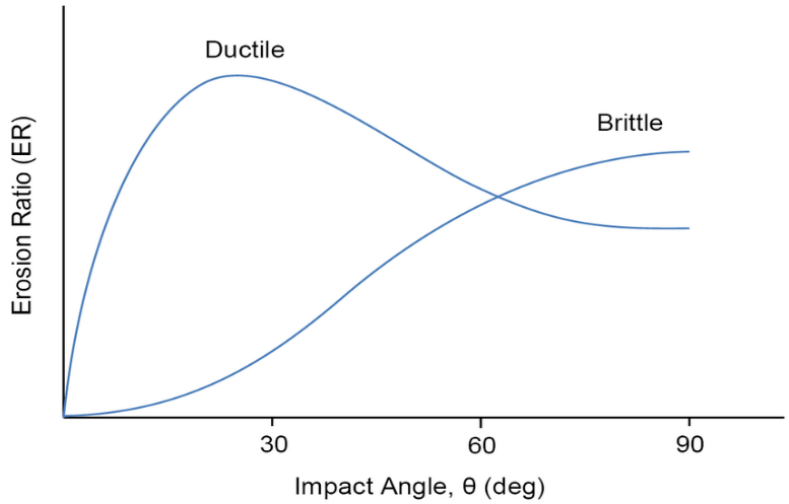

Figure 2. 4 Variation of erosion ratio with impact Angle for ductile and brittle materials [3]

2.3.3 Particle Properties

The erosion rate is greatly influenced by particle properties such as size, shape, and hardness. The influence of particle characteristics on erosion rate has been studied extensively, although the implications are still unclear. Tilly [32] in 1973 figured out the effect of particle size on erosion rate. The result in Figure 2.5 depicts the impact of particle size on erosion rates. For smaller groups, it was shown that when the particle size is increased, the erosion rate increases dramatically. This substantial increase in kinetic energy is attributed to this observation. When it comes to the mass loss ratio, it remains constant as the particle size is increased beyond a threshold point. This behavior was shown to be influenced by particle size, the number of particles impacting the surface, particle kinetic energy, and entanglement between entering and rebounding particles. Finnie and Misra [29] in 1981 observed the same pattern and determined the critical particle size to be 100 micrometers.

Oka [38] in 2005 discovered a power law relationship between particle size and erosion rate. The particle size exponent in Oka's erosion model is 0.19. Levy et al. [33] in 1983 studied the effect of particle hardness on erosion rate. Because weak particles (calcite and apatite) break into many fragments as they impact the surface, erosion rates for these

weak erodents are relatively low. However, the erosion rate stays constant for particles having a Vickers hardness of roughly 700 HV. These particles are powerful enough to fracture the target surface when they collide with it. In addition, Arabnejad et al. [40] in 2015 found that particle hardness and erosion rate have a power law relationship. The exponent of Vickers hardness, according to the test data, is 0.89. It is difficult to understand how particle form affects the erosion rate. Levy and Chick [33] in 1983 examined AISI 1020 steel with spherical and angular steel particles to better understand the effect of particle form on erosion rate. The erosion rates of angular particles were found to be four times higher. They also talked about how spherical particles make shallow, rounded craters, whereas angular particles make sharper, deeper craters. As a result, angular particles are more capable of eliminating mass.

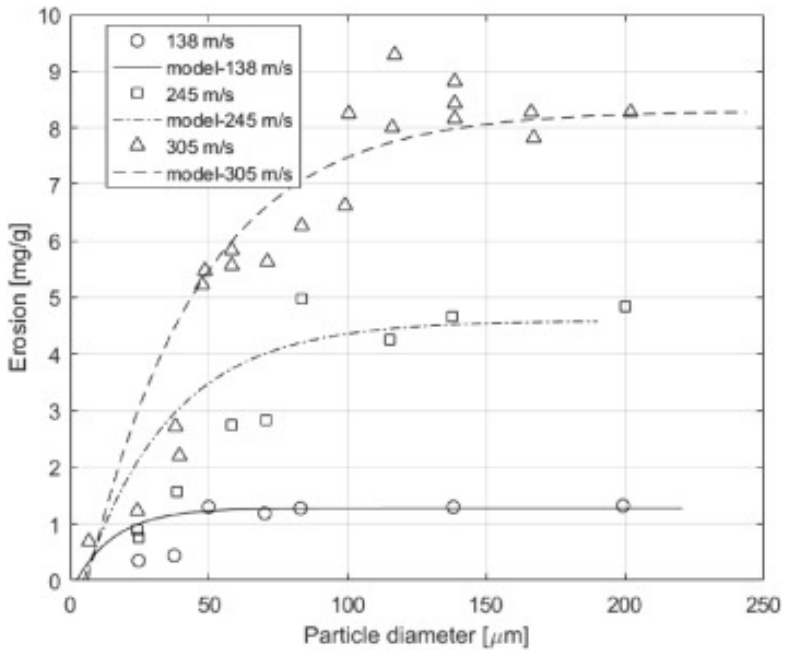

Figure 2. 5 Erosion rate Cr steel as a function of quartz particle size velocity

2.3.4 Particle Concentration

Many researchers studied the effect of particle concentration on erosion rate. They all came with results that erosion rate decreases by increasing erodent concentration due to an increase in particle-particle interaction which lowers the kinetic energy and leads to ductile material elastic deformation [41]. This interaction becomes dominant particularly when concentration drops to a dilute mixture Using numerical methods, Nguyen et al. [42] investigated the influence of sand erodent concentration on materials degradation rate and found out that erosion rate reduces by increasing the sand particle concentration.

Wang et al. [43] in 2017 performed erosion tests by changing particle flux from 1 to 8 percent by weight. He displayed a power-law relationship between erosion rate and slurry concentration. (See equation 2.2).

$$\text{ER} = \frac{k}{\emptyset^{0.19}} \tag{2.2}$$

k is a constant, and φ is the solid particle volume fraction in the fluid.

Using a direct impact test, Alam [44] looked at solid particle degradation in five different types of steel. According to Figure 2.8, the normalized erosion rate of targeted material increases with erodent concentration. More material was removed from the targeted surface when the erodent concentration was high.

2.3.5 Erodent Viscosity

Alamu [45] revealed that the flow structure becomes more periodic when fluid viscosity increases. In the sand erosion mechanism, the erosion rate decreases by using less viscous liquids. It is due to the formation of a protective sliding bed at the bottom of pipelines.

2.3.6 Properties of the Eroded Material

Researchers looked at several attributes of the base material, like toughness, stiffness, flexibility, strain stiffening, and thermal characteristics, to determine how they related to erosion rate. Vickers hardness is a material characteristic that has a significant impact on erosion rate. In 1972, Finnie et al. [29] discovered a link between work annealed material volume loss and Vickers hardness. Equation 2.3 shows this relationship between volume loss and Vickers hardness of work material.

$$\text{Volume loss} \propto \frac{1}{Hv} \tag{2.3}$$

He also noted that an increase in Vickers hardness of steel by heat treatment does not affect erosion rate. Oka et al. [38] in 1993 researched to see the relationship between surface hardness and erosion damage. It was discovered that as the indentation size increases for all test materials, Vickers hardness, Hv, decreases. In addition, Arabnejad et al. [40] in 2015 conducted multiple erosion tests and discovered the following relationship between cutting erosion rate and annealing Vickers hardness:

$$\text{E}R_c \propto \frac{1}{\sqrt{Hv}} \tag{2.4}$$

Here, ERc denotes cutting erosion rate, and Hv represents Vickers hardness.

2.4 Types of Erosion Tests

Researchers employ a variety of erosion test rigs to assess erosive wear under various operating situations. The erosion mechanism is the same in all of the erosion test rigs the various types of test rigs are explained in this article.

2.4.1 Slurry Pot Erosive Wear Test

Clark [35] in 1991, Desale [18] in 2008, and Lindgern [46] in 2014 employ a slurry pot erosion tester to investigate the wear resistance of various materials. A slurry pot has the advantage of being straightforward to use for material grading of erosion resistance. However, the turbulence created inside the pot and the variations in concentration make it impossible to apply the test data for quantitative analysis. The schematic of a slurry pot erosion tester is shown in Figure 2.6. A pot and a revolving shaft make up this device. On the shaft, test samples are mounted. To give the appropriate rotational velocities, the shaft is coupled to a motor. To guarantee that the slurry is well mixed, baffles are affixed to the inner wall of pot. To investigate the effect of the orientation angle on erosion behavior, flat test samples can be employed and tilted.

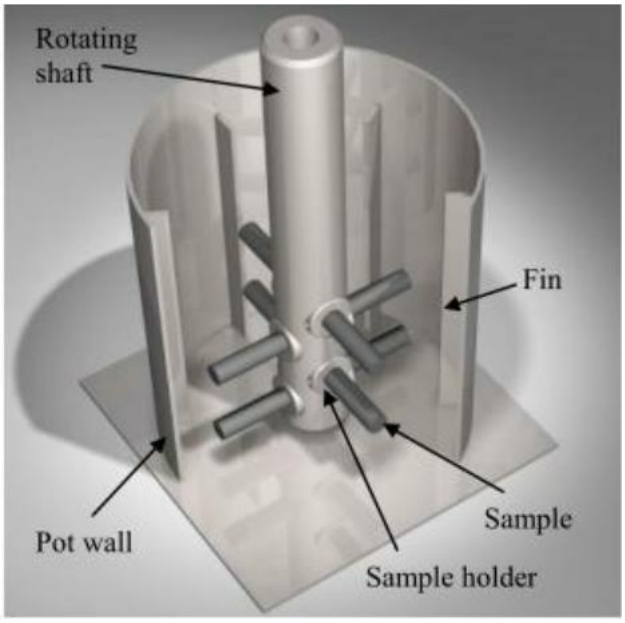

Figure 2. 6 schematic of slurry pot tester

2.4.2 Direct Impact Test

In erosion studies, the direct impact or impinging jet test is most used because it provides more control of particle impact speed and particle impact angle. At the exit of the nozzle,

the air compressor provides the desired air speed by regulating air pressure. Sand particles come out of the sand feeder due to this air speed. The air flow mixtures strike the targeted surface in a repeated manner. As a result of it, the material gets eroded. In this method, the impact angle can be varied very easily by rotating the specimen holder. Figure 2.7 represent the schematic of the direct impingement jet test with the air-sand flow.

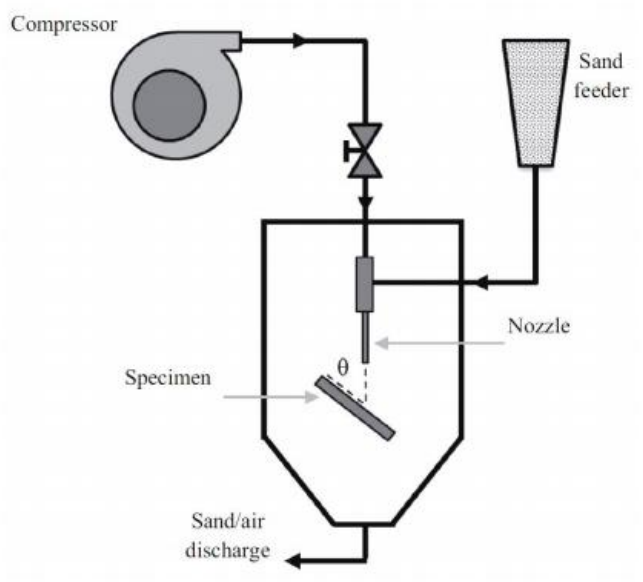

Figure 2. 7 Schematic of Direct impingement set

2.4.3 Coriolis Test

Tuzson [47] in 1984 developed another technique for measurement and simulation of erosive wear of the targeted surface with grazing angles. It is known as the Coriolis slurry erosion test. It is common in abrasive pumps, pipelines, and cyclone separators. Figure 2.8 illustrates a schematic of Coriolis slurry erosion tester. The fundamental disadvantage of this test is that abrasive particle velocities within the channels cannot be precisely determined.

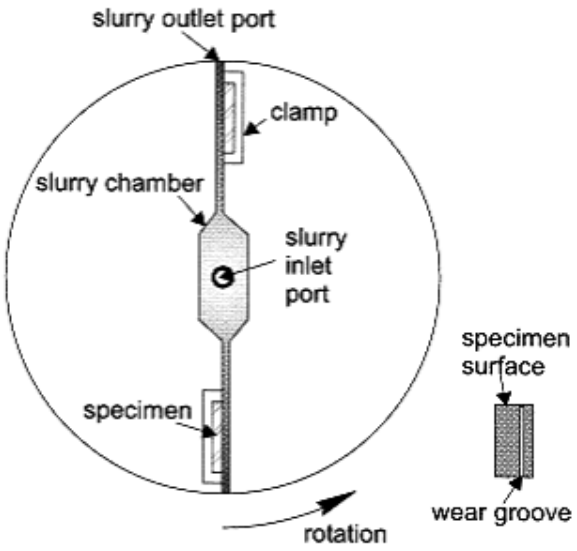

Figure 2. 8 Schematic of Coriolis slurry tester

2.4.4 Flow Loop Test

Some studies in the literature have been carried out to determine the rate of erosion in pipelines or bends. The pipe loop test simulates operational circumstances and enables for measurement of erosion in both single-phase and multi-phase flow. Kesana [48] in 2013 and Vieira [49] in 2014 assessed the erosion damage happening in slug and annular flow regimes respectively at the Erosion/Corrosion Research Center (E/CRC). For erosion measurements in the bend, ER probes and ultrasonic sensors are commonly utilized. Although this erosion test is valuable for determining the erosion rate and region of maximal thickness loss in operational settings, regulating particle impact speed and angle is extremely challenging. So, because particle impact velocity and inclination can be measured with the impinging jet, it is an appropriate test method. This equipment, on the other hand, is incapable of producing particle collisions at an incredibly low impingement angle (less than 5 degrees). The Coriolis test works well at a lower impingement angle however flops at high degrees. Even though the slurry pot tester can generate a huge spectrum of impingement angles, the particle impact speed cannot be estimated because of too much turbulent flows within the pot. Additionally, the concentration distribution within the tank varies. As a result, the proper apparatus should be selected based on the research. Figure 2.9 shows a schematic diagram of the slurry erosion test loop.

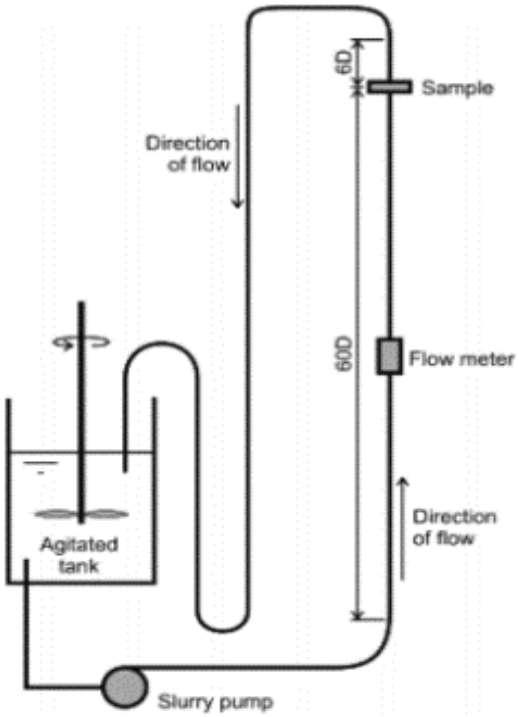

Figure 2. 9 Schematic of slurry erosion test

2.5 Solid Particle Erosion Models

Three different erosion models are discussed in this section. These models are developed to predict the erosion rate, which is necessary to minimize the degradation risk in production systems. Some models are based on empirical correlations with laboratory data and include numerous simplifying assumptions, whereas others include built-in mechanistic modeling of the different physics and mechanisms of erosion.

2.5.1 Mechanistic Erosion Models

Various mechanistic models have been created to predict the degree of erosion, which is required for determining the equipment's expected lifespan and improving the design. Many oil producers have historically relied on API Recommended Practice 14E (API RP 14E), which recommends a production velocity of Ve [ft/s] as the maximum production velocity to prevent major erosion concerns. Equation 2.5 represents this limiting production velocity.

$$\mathrm{Ve} = \frac{C}{\sqrt{\rho_m}} \tag{2.5}$$

Where C is an empirical constant and ρ_m [lbs/ft3] is the fluid mixture density. API RP 14E guideline suggests C=100 for continuous services and C=125 for intermittent services.

Although equation 2.5 is straightforward to apply, it has the flaw of failing to consider several important aspects of the erosion mechanism. Failure to consider essential components in erosion rate might lead to erroneous equation estimations, according to Shirazi et al. [50]. In addition, in 2000, McLaury et al. [51] compared field failure data to API RP 14E erosion projections and found that the recommendation overpredicts degradation.

In other words, field data indicate that the empirical equation of API RP 14E is conservative. Researchers developed several alternative mechanistic models to alter the API RP 14E recommendation. For erosion rate prediction, Salama and Venkatech [52] in 1983 suggested a closed-form equation. Equation 2.6 was developed by these two researchers.

$$\text{ER} = S_m \frac{WV^2}{D^2} \tag{2.6}$$

Where ER is the erosion rate in mpy, W is the sand rate in lb/day, V is fluid flow velocity in ft/s, D is pipe diameter in inches, Sm is a geometry-dependent constant, and the following values are suggested for that:

Svendeman and Arnold [53] (1994) proposed a similar equation, although different values for Sm were reported: Later, Salama [54] (2000) developed a new erosional velocity limit Ve [m/s] for sand-laden flows. Where *D* is the pipe diameter in mm, *W* is sand flow rate in kg/day, ρ_m is the fluid mixture density in kg/m3.

Shirazi et al. [50] (1995) proposed a method for calculating the single-phase flow penetration rate in elbows and tees. Unlike prior models, this mechanistic model considered a variety of variables, including geometry type, size, and material; fluid characteristics (density, velocity, and viscosity), and sand sharpness, density, and rate. The following is the mechanistic model:

$$\text{H} = \text{Fm Fs Fp Fr/d} \frac{WV_L^{1.23}}{\left(\frac{D}{D_o}\right)2} \tag{2.7}$$

McLaury et al. [51] (2000) devised a novel mechanistic model for solid particle degradation in multiphase flow. Mazumdar et al. [55] (2005) modified the previous mechanistic model at E/CRC by taking into account more aspects of different multiphase flow patterns. Even though mechanistic models are simple and easy to use, their

reliability pales in contrast to CFD-based estimates. Additionally, mechanistic models are limited to a certain shape and are not relevant in all cases.

2.5.2 Theoretical Erosion Equations

Researchers have established many mathematical models to predict degradation intensity as a function of particle impact conditions and material characteristics. Finnie's [29] equation was among the first to be published in the journals (1960). In this model, a single particle should contact the layer at an inclination determined from the surface. It's also possible that the particle removes the material through a cutting process. The abrasive particle does not break apart following impingement because it is harder than the target surface. Material is removed in a way like that found in machine tools, and the target surface is expected to flex plastically. Based on these assumptions, Finnie [29] (1960) constructed an equation for calculating the quantity of material eliminated by sand particles W. The last phrase is as follows:

$$w = c\frac{MV^2}{\Psi pK}\left[\sin[2\alpha] - \frac{6}{K}\sin -2(\alpha)\right] \tag{2.8}$$

$$w = c\frac{MV^2}{\Psi pK}\left[\frac{K\cos^2(\alpha)}{6}\right] \tag{2.9}$$

Where K is the ratio of vertical to horizontal frictional force and is the ratio of contact depth to cut depth. K=2ss was proposed by Finnie [29] (1960). V is the eroding surface flow stress, M is the total mass of abrasive particles, and p is the particle impact velocity. Furthermore, it is believed that half of the particles are equally efficient as the single perfect particle. As a result, Finnie chose C=0.5 at random. Finnie [29] (1960) used experimental data on aluminum, copper, and steel erosion to compare model predictions with experimental data. At low impact angles, when the cutting process is prominent, the model may forecast erosion. However, at high impingement angles, it fails to forecast degradation. The plastic deformation process, which was not taken into consideration in Finnie's model, is to blame for the discrepancy between model prediction and experimental evidence.

Finnie's model was updated by Bitter [8] (1963), who proposed that the cutting and deformation operations occur concurrently. At high impingement angles, according to Bitter, the cutting mechanism is minimal, and the deformation mechanism takes over. Bitter [8] (1963) discovered that heavy hits at high impact angles cause plastic deformation and developed a mathematical formula to explain it.

$$E_d = \frac{1}{2}\frac{M(V_P \sin\theta - V_n)^2}{\varepsilon_b} \quad (2.10)$$

Where Ed denotes deformation volume loss, M denotes the total mass of hard particles, and Vn is the standard element particle speed under which erosion harm does not occur. The power required to reduce a unit quantity of material due to deformation is known as the deformed wear factor. Figure 2.10 shows Volume Removal Variation with Impact Angle.

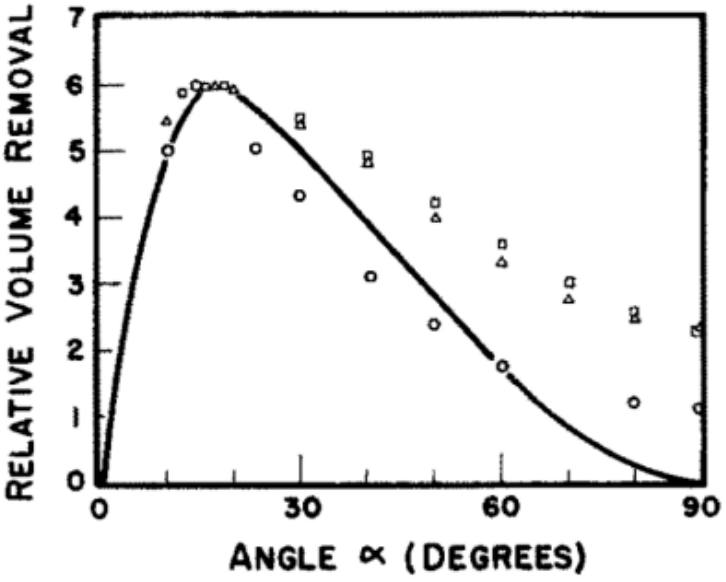

Figure 2. 10 Volume Removal Variation with Impact Angle (Solid Line) - Experiment Data Points for Copper, SAE 1020 Steel, and Aluminum

2.5.3 Empirical Erosion Equation

Several equations based on practical experiments have been created in addition to theoretical erosion equations. Most of these erosion equations have been published in Finnie's (1960) generic form:

$$\text{ER} = KV_p^n \, j\,(\emptyset) \quad 2.10$$

The erosion ratio (ER) is the ratio of material mass loss to the mass of erodent particles. K is a constant defined by the properties of the specimen. Vp is the particle impact velocity, which follows a power law relationship with wear rate. When particles collide with the area at low impact angles, f (θ) provides material surface cutting; when particles collide with the surface at high impact angles, f (θ) accounts for the removal of material through the deformation mechanism. Ahlert [56] (1994) and McLaury [51] (1996) proposed Equation 2.10 as a carbon steel and aluminum erosion equation at the E/CRC.

The value of 1.73 was proposed for n based on the experimental experiments. A function for calculating impact angles was also provided, having the following form:

$$f(\emptyset) = a\,\emptyset^2 + b\emptyset^2 \qquad 2.11$$

2.6 Summary

This chapter provided a thorough examination of solid particle erosion mechanics and significant factors impacting erosion rates. Various sorts of degradation tests were also briefly outlined. This chapter also offered numerous mechanical methods for degradation predictions in simple geometries. However, complicated down hole configurations that are of importance to oil and gas companies are not covered by conventional mechanistic models.

CHAPTER 3:

METHODOLOGY

3.1 Introduction

This chapter explains the research methodology used in the present research. It consists of six sections. Section 3.1 is the introduction of the research methodology. Section 3.2 of this chapter is experimental details which comprise detailed information regarding the work material used in tests, experimental setup and its fabrication, experimental conditions, and sample preparations. Section 3.3 covers the 3D modeling of the experimental setup. Section 3.4 is about experimental procedures and test matrices. Three parameters were varied during testing. These variable parameters were (1) impact velocity (2) impingement angle (3) particle size. Section 3.5 describes the analysis approaches applied during experimentation. Mass loss analysis, microscopic imaging approach, scanning electron microscopy, computational fluid dynamics modeling, and simulations are brought into services for developing and modification of erosion models. A microscopic imaging approach was used to comprehend the erosion microstructure. Section 3.6 gives a summary of the methodology adopted for this research. The overall research approach is shown in figure 3.1.

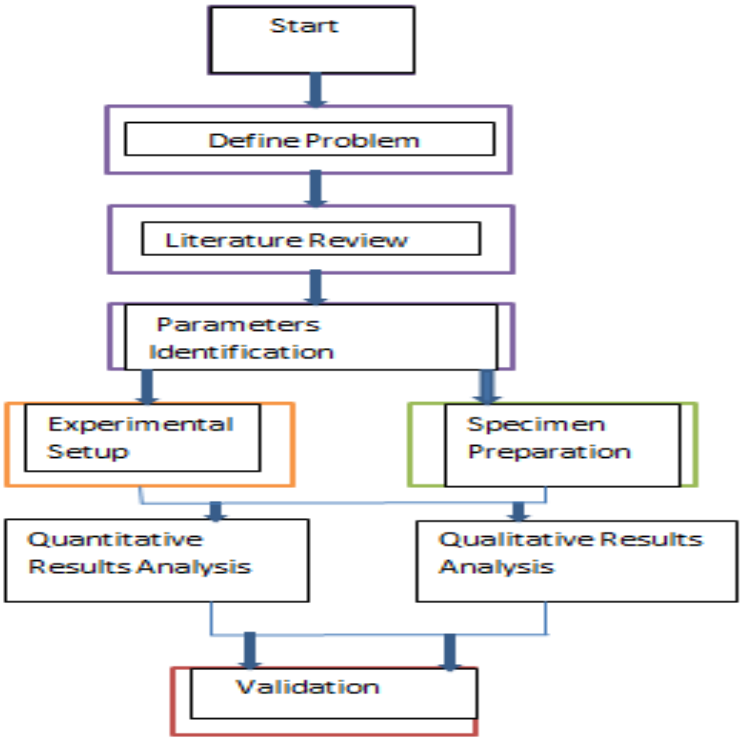

Figure 3. 1 Overall research approach

3.2 Construction of CAD model

The 3D model of the experimental setup was constructed by using SOLIDWORKS 2019. The development of this model is explained in detail in the following sections.

3.2.1 Control valve

The controller was made by first making a rectangle for the base, extruding the rectangle, and making the cuboid. After this, the circle of various sizes was made and extruded on opposites of the cuboid to make the input nozzle and output side. The upper circle was first made in large size, extruding, then making a smaller size circle and extruding, alternating this to make the control.

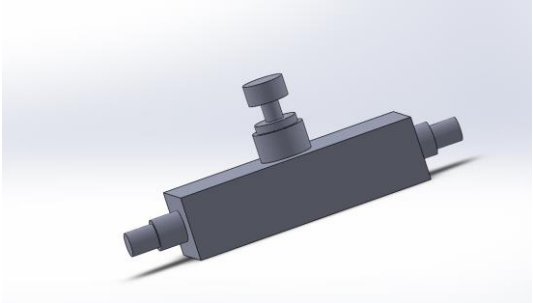

Figure 3. 2 control valve

3.2.2 Water tank

First, the base cylinder was made with the help of a circle and extruding to make a cylinder. This was further made by using a revolving extrude along the center of the cylinder to make the conical extrude. Then a circle is made to provide the tip of the tank and a fillet was made on both sides to provide a clean and proper finish.

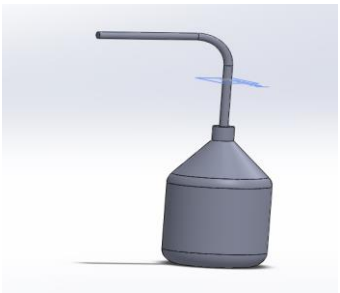

Figure 3. 3 Water tank

3.2.3 Pipe

The pipe was made with the help of swept boss extrude by initially making a smaller sketch with the help of line and then making the circular extrude, the fillet of the sketch is made to make curves in the design of the pipe to further aid in the assembly process.

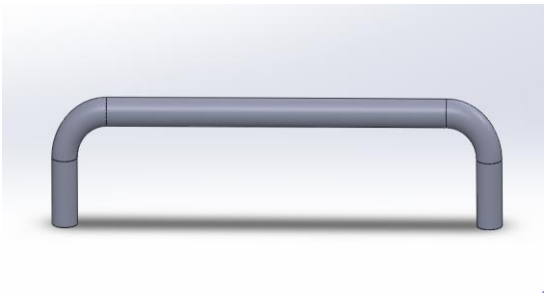

Figure 3. 4 Piping

3.2.4 Sand feeder

The holder is an assembly part made in several steps; the first part is the stand itself which makes the base of the assembly. This is made with the help of first making the rectangle then making another rectangle on the already existing cuboid and extruding that to further make the stand and doing the same for the other parts of the stand. The bottle was initially made by the cylinder with help of extruding from a circle of the particular dimensions that the extrude cut was made in the stand. The further design was made by filleting the edges of the cylinder and then making circles of various dimensions to extrude making the tip on top of the bottle. These parts were then assembled.

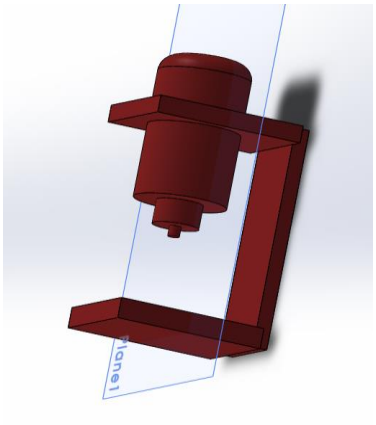

Figure 3. 5 Sand feeder

3.2.5 Mixing nozzle

The 2 to 1 joiner is made with a combination of circle extrude as well as making circles of various extrude to various degrees to result in proper input and output nozzles for both 2 and 1 ended input and output sides.

Figure 3. 6 Mixing nozzle

3.2.6 Nozzle

The nozzle was initially made with the help of a circle and extrude that enables the creation of the primary cylinder, with further work that can be done by the making a sketch on one side of the cylinder and then using the circular linear pattern will be used to replicate it across the outer edges of the cylinder. Then using extrude cut is used to cut out the required parts.

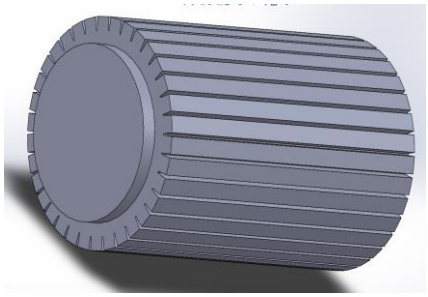

Figure 3. 7 Nozzle

3.2.7 Table

Similar to the stand made in the assembly part above, the table will be made similarly and will include the use of the first sketch to make the rectangle of the required length and then using the extrude to provide depth. Then the use of sketch on the surface of the table will be implemented and all the sketches will be squares of equal dimensions and then extruded to larger depths to provide the legs for the table.

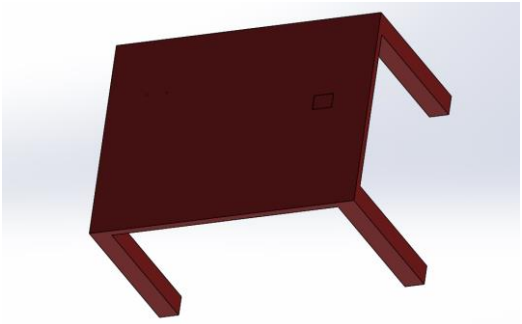

Figure 3. 8 Table

3.2.8 Pump

The pump was made primarily from a combination of the rectangle along with the use of extrude boss, revolve, circular, and making sketches on all surfaces. The first thing was the usage of the rectangle and extrude. The next thing was the usage of sketch on various sides of the cuboid that will correspond with the creation of cylindrical and cuboid creation on both all sides. Specified parts were filleted for required changes and the hooks were made with more sketches along with small depth to provide the needed design.

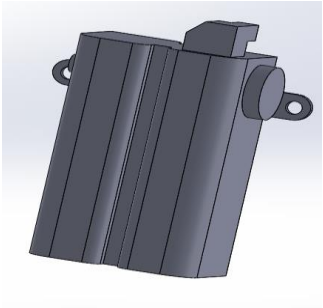

Figure 3. 9 Pump

3.2.9 Holder Assembly

The assembly for the stand is made by first creating a stand on the base. This will be done in a process like a stand that will make the stand with a strong and large base with the other part made with a similar manner but the extrude cut will be made following the design requirements of the Project.

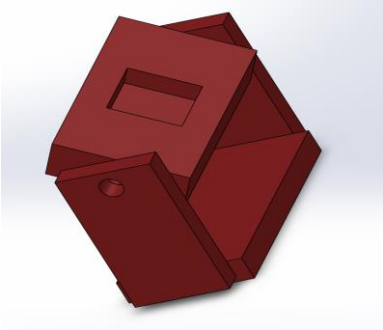

Figure 3. 10 Specimen holder

3.2.10 Final Assembly

The final assembly of the project will be done with the aid of other parts of the assembly that will be included in the final SLDASM file. This will include all the files in the already made SLDPRT files, i.e., the nozzle, the stand, the pump, and various others. The core idea of this assembly is to assemble all these files in such a way that they are all fixed on the table solid part.

The first part of this is to make changes to the table to make sure that all parts of the assembly can fit properly. This included with hooks and design anchors to set other parts on the table as seen on the table. Then the other parts will be inserted into the assembly file. Then using mate, various pieces of the assembly will be attached, with parts being attached in between each other with the help of small and large pipes and ultimately creating the final product as shown in the figure.

The other details of the project were implemented with the addition of various colors added with the help of appearance changes being given different coloring patterns to help aid in the differentiation of different parts such as pipe, pump, and stand. The tank was also attached via a pipe to the bottom of the table with mates similar to other parts.

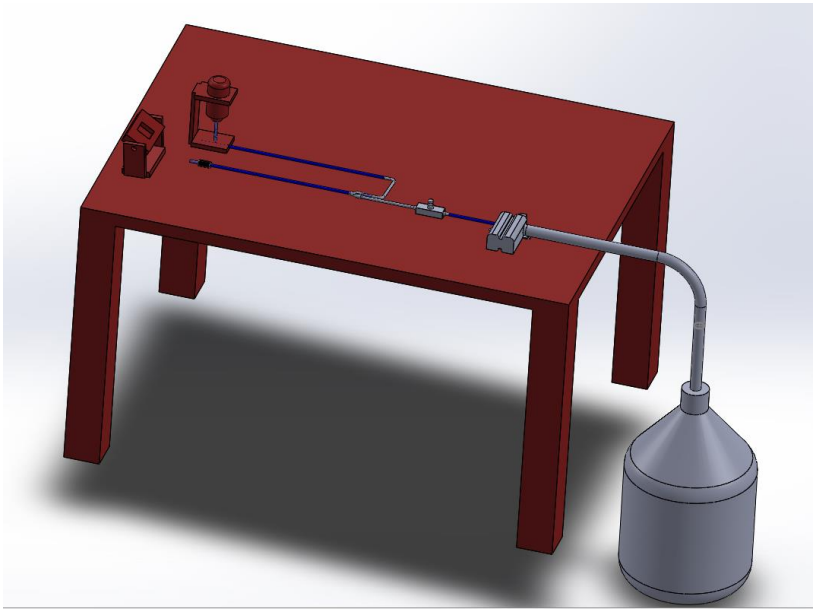

Figure 3. 11 Final 3D assembly

3.3 Experimental Details

This section describes the specifics and functions of all parts of an experimental setup. These parts include work material used, tool, machines and devices, water tank, input and output pipes, sand carrier and water recycling pipes, centrifugal pump, sand feeder, test specimen holder, control valve, dc power supply, three ways mixing nozzle, exit nozzle, sand collector and water recycling box.

3.3.1 Specimen Material

The test specimen AISI 1018 carbon steel with a hardness value of 168 ± 7 HV was employed in jet impingement tests. It was used because of its necessitated application in

the industrial sector. Tables 3.1 show the elemental composition and mechanical properties of specimen material respectively.

Table 3. 1. Composition and mechanical properties of specimen

1018 CS								
Si	Cr	Cu	P	C	S	Ni	Mn	Fe
0.26	0.21	0.25	0.045	0.2	0.035	0.3	0.52	Balance

3.3.2 Specimen geometry and dimension

A flat plate of specimen was employed. It was in square shape with thickness of 3 millimeters and length of 60 millimeters. This configuration was used because of three main reasons (1) elbow shaped specimens were difficult to paint (2) most erosion models were developed on flat plate configuration (3) results with flat shape plates can be correlated with elbow shape plates because of testing at different angles. Figure 3.2 shows a specimen used in testing.

Figure 3. 12 A specimen used in testing

3.3.3 Specimen Preparation

A square sheet of 3160 millimeters length and 3 mm thickness was cut with wire electro discharge machining. Grinding was done to achieve surface finish. For this purpose, a 6 Inch 150mm 9P fiber polishing buffing wheel of nylon was used. Figure 3.3 shows this buffing wheel. Figure 3.4 shows plate after grinding. Then half plates were painted using three different layers of paint (1) red paint (2) yellow paint (3) grey paint. All of them were fast drying spray paints of MUBAH company. Figure 3.5 (a) shows red paint, figure 3.5 (b) shows yellow paint and figure 3.5 (c) shows grey paint used in multilayer painting. Red paint is more ductile than yellow and grey paints. It is easy to remove less ductile paint as compared to high ductile paint. That is why bottom most layer was of red paint while topmost layer was of grey paint. Figure 3.6 (a) shows plate after painting first layer,

figure 3.6 (b) shows plate after painting second layer, and figure 3.6 (c) shows plate after painting third layer. Rest of plates was mirror polished. Figure 3.7 shows plate after mirror polishing. Specimens were then cleaned with ethanol, dried with a heat gun, and placed in silica gel to avoid moisture exposure before the tests. Figure 3.8 (a) shows ethanol, figure 3.8 (b) shows heat gun, and figure 3.8 (c) shows silica gel which were used to clean, dry and preserve the specimen.

Figure 3. 13 6 Inch 150mm 9P fiber polishing buffing wheel of nylon

Figure 3. 14 Plate after grinding

(a) **(b)** **(c)**

Figure 3. 15 Paints used for multilayer painting (a) red paint (b) yellow paint (c) silver paint

(a) (b) (c)

Figure 3. 16 Plates after painting (a) plate after red layer painting (b) plate after yellow layer painting (c) plate after silver layer painting

Figure 3. 17 Mirror polished plate

(a) (b) (c)

Figure 3. 18 Other things used in testing (a) ethanol (b) heat gun (c) silica gel

3.3.4 Water Tank

A bottle of 19-liter volume was used as a water tank. It was used to provide and restore water continuously. Figure 3.9 shows water tank used in testing.

Figure 3. 19 Water tank used in testing

3.3.5 Input and Output Pipes

Input pipe of 12 mm diameter was used. It was made of blue nylon material. One end of pipe was dipped into water tank while other end was joined with input of centrifugal pump. Centrifugal pump sucked water through this pipe. While output pipe of 8 mm diameter was used. It was also made of blue nylon material. One end of this pipe was connected to outlet of centrifugal pump while other end was joined with control valve. It carried water from centrifugal pump to control valve. Figure 3.10 (a) shows input pipes, and figure 3.10 (b) shows output pipes

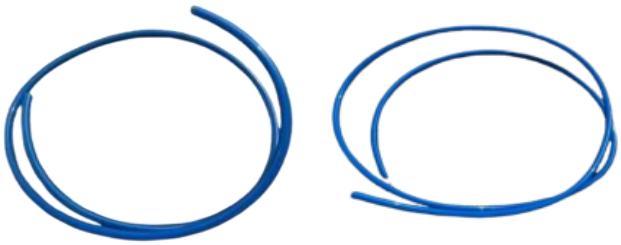

(a) (b)

Figure 3. 20 Pipes used in experimental setup (a) input pipe (b) output pipe

3.3.6 Sand Carrier and Water Recycle Pipes

Both sand carrier and water recycle pipes were of 8 mm diameter. Both pipes were made of blue nylon material. One end of sand carrier pipe was linked with sand feeder while another end was joined with three way mixing nozzle. Sand transportation occurred through this pipe from sand feeder to three ways mixing nozzle. Sand mixed with water in three ways nozzle and hit the targeted material. Recycling pipe was used to recycle water and to save wastage of water. One end of this pipe was connected with covering box while other end was dipped into water tank. Figure 3.11 (a) shows sand carrier pipe, figure 3.11 (b) shows water recycle pipe.

(a) (b)

Figure 3. 21 Other pipes used in experimental setup (a) sand carrier pipe (b) water recycle pipe

3.3.7 Centrifugal Pump

A dual motor high pressure pump of EARTH company was used in testing. It was consisted of three wires. One wire was of positive terminal while other two were of negative terminals. This pump is able to deal with water only. Properties of this pump is given in Table 3.2.

Table 3. 2 Properties of centrifugal pump used in testing

Pressure (Psi)	Flow Rate (L/min)	Voltage (V)	Current (A)
220	7 to 9	12	2.5 to 6

Figure 3.12 shows the centrifugal pump used in testing.

Figure 3. 22 A centrifugal pump

3.3.8 Sand Feeder

Sand feeder was consisted of sand container and wooden holder. Sand container was a simple plastic bottle of 1 liter volume. Sand carrier pipe was connected to this bottle through hole of 8 mm diameter. Electron gum was used to connect the sand carrier pipe

with sand container. Wooden holder was used to clasp the sand container. Wooden holder was made with three wooden pieces joined together with the help of nails. A hole was drilled into wooden holder corresponding to diameter of sand container. Figure 3.13 shows glue gun, and figure 3.14 shows sand feeder used in testing.

Figure 3. 23 A glue gun

Figure 3. 24 A sand feeder

3.3.9 Test Specimen Holder

A wooden test specimen holder was used. It was consisted of five wooden pieces which were joined together by using nut and bolts. It was rotatable with square cavity which was created by using CNC machine. A cavity was of 50 millimeters length and 50 millimeters width to accommodate 50 millimeters length and 50 millimeters width of targeted material. Rest area of specimen was not exposed to slurry. For each experiment, nuts were escaped, and new specimen was placed inside the cavity. In this way, all experiments were conducted. Figure 3.15 shows the test specimen holder used in experimental setup.

Figure 3. 25 A specimen holder

3.3.10 Control Valve

A control valve of 8 mm input and 8 mm output was used to decrease the flow of water. A knob was on its head which was rotatable and controlled the flow of water. Figure 3.16 represents the control valve.

Figure 3. 26 A control valve

3.3.11 DC Power Supply

A dc power supply was also used to control the flow rate of water. Flow rate was controlled by varying the input voltage of power supply. Its voltage range was from 0V to 14 V. Figure 3.17 shows dc power supply.

Figure 3. 27 A dc power supply

3.3.12 Three Ways Mixing Nozzle

Three ways mixing nozzle was used in experimental setup. It was having two inlets and one outlet. One inlet was for water while other was for sand. Outlet of it was connected with the nozzle through 8 mm pipe. The function of it was to mix sand and water and send slurry to nozzle. Figure 3.18 shows three ways mixing nozzle.

Figure 3. 28 A three ways mixing nozzle

3.3.13 Exit Spray Nozzle

Exit spray nozzle of 2mm diameter was used in an experimental setup. It was used to provide jet of slurry to specimen. Small diameter means there will be large velocity at exit of nozzle. Figure 3.19 shows an exit spray nozzle.

Figure 3. 29 An exit spray nozzle

3.3.14 Sand Collector and Water Recycling Box

It was a wooden box used to collect sand and to save wastage of water by recycling it. The benefit of using this box was to decrease the need of both sand and water. Figure 3.20 shows the sand collector and water recycling box.

Figure 3. 30 Sand collector box

3.3.15 Erodent

Two different sized natural fine silica sand particles were used as erodent during testing. Silica fine sand particles were of 53 microns and 63 microns. These fine sand particles were filtered from big sized simple sand using two sieve meshes of 270 and 230 respectively. Fine particles of silica sand were used because there was a little research on erosion due to these particles. Figure 3.21 (a) shows simple sand, figure 3.21 (b) shows 53 microns fine sand, and figure 3.21 (c) shows 63 microns fine sand. Table 3.5 represents the chemical composition of sand fines.

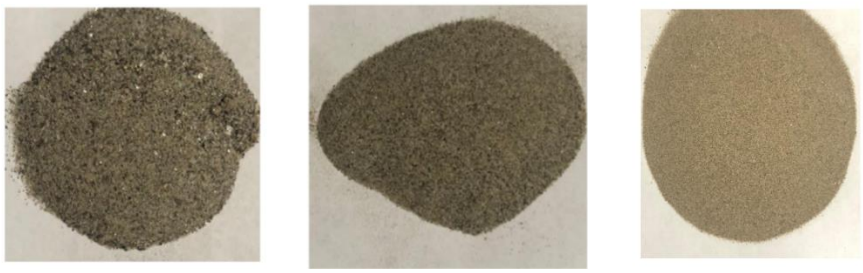

(a) (b) (c)

Figure 3. 31 Three different sized sand particles (a) simple sand (b) 63 microns particles (c) 53 microns particles

3.3.16 Sieve Meshes

Two different sized sieve meshes were used to filter the fine sand particles of 53 microns and 63 microns. These meshes were bought from market according to an ASTM standard. For example, 53 microns sieve mesh has 270 holes in 1 square inch area while 63 microns sieve mesh has 230 holes in 1 square inch area. Figure 3.21(a) shows 53 microns sieve mesh, and figure 3.22 (b) represents 63 microns sieve mesh. Table 3.4 shows the relationship between ASTM standard and size of sieve mesh in microns.

(a) (b)

Figure 3. 32 Two different sized sieves mesh (a) 53 microns sieve mesh (b) 63 microns sieve mesh

Table 3. 3 Relationship between ASTM standard and size of sieve mesh in microns

ASTM 11-70 MESH	OPENING IN MICRONS
5	4000
6	3300
7	2600
8	2400
10	2000
12	1600
14	1400
16	1250
18	1180
20	1120
25	1000
30	850
35	710
40	600
45	500
50	420
55	355
60	300
65	250
70	210
80	180
100	150
120	120
150	105
170	90
200	75
230	63

270	53
325	45
400	37
-	25

3.3.17 Complete Experimental Setup

Figure 3.23 shows complete experimental setup. It was locally fabricated to study erosion of steel due to wet sand particles impact. It was consisted of all above explained 16 components. Each component was designed or chosen by doing some required mathematical calculations. For example, our goal was to conduct experiments at different angles of specimen with respect to nozzle, so we designed a rotatable test specimen holder. Similarly, we wanted to use two different sizes of fine particles, which is why we used two different sized sieve meshes of 53 microns and 63 microns. In the same way, we selected a pump according to our requirements. Sand collector and water recycling box was used to avoid wastage of water and sand. Three ways mixing nozzle was used to mix sand with water. Exit nozzle was used to produce jet of required velocity. Both qualitative and quantitative analysis was performed using this experimental setup.

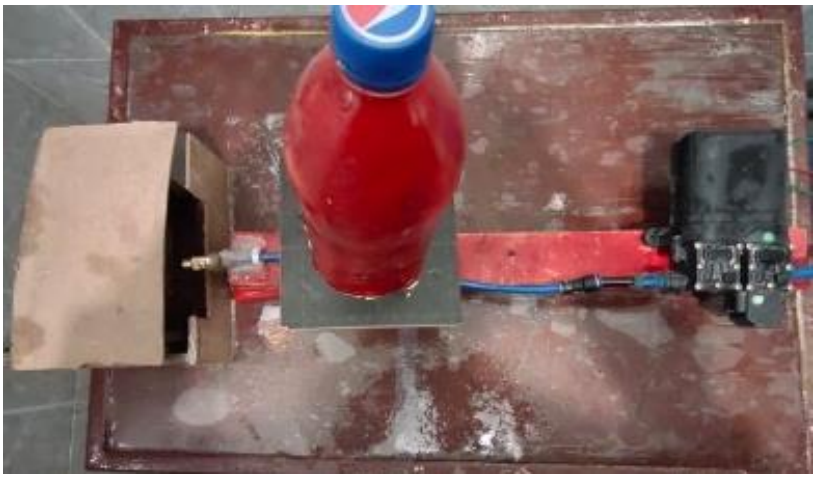

Figure 3. 33 A complete experimental setup

3.4 Experimental Procedures and Test Matrices

Experiments were divided into two different categories. Half experiments were done for multilayer painted specimens while other was done for mirror polished targeted materials. Mass loss was determined in mirror polished case while a qualitative approximation of erosion distribution was obtained in multilayer painted specimen. There were chosen three variable parameters to conduct these experiments. These variable parameters were

(1) impact velocity (2) impingement angle (3) particle size. Particles concentration and standoff distance were remained same during all experiments. Particle concentration was 2 % while standoff distance between exit nozzle and test specimen was 5 cm. Figure 3.34 illustrates a piping and instrumentation diagram (P&ID) of the experimental apparatus used for testing.

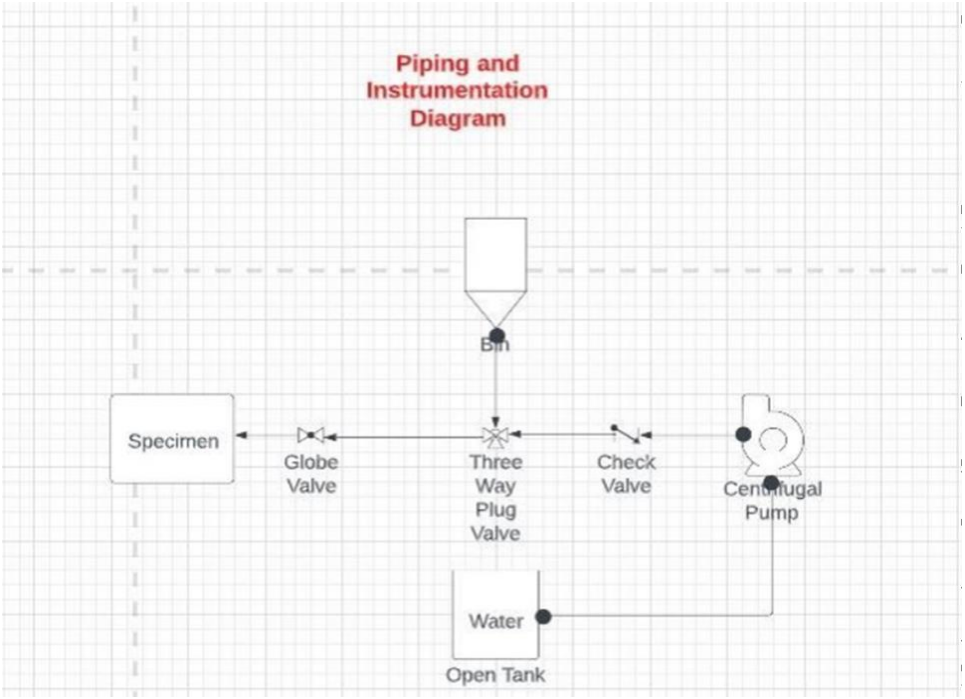

Figure 3. 34 A Piping and Instrumentation Diagram (P&ID)

As flow meter was not used, so flow rate was measured experimentally. Time was noted by using stopwatch for filling 1 liter of water bottle. Then velocity was calculated by using equation of continuity and desired velocity was obtained by employing iterative process. Equation 3.1 is equation of continuity which gives relation of flow rate with flow velocity and area of flow passage.

$$Q = AV \tag{3.1}$$

Diameter of exit nozzle was 2 mm. Area was calculated by using equation 3.2 which gave value of 0.00001256.

$$A = \pi r^2 \tag{3.2}$$

After adjusting the power of pump by using dc power supply, specimen was placed at required angle. Then system was turned ON. For multilayer painted steel plates, test time was 30 minutes. For mirror polished specimens, test time was 2.5 hours to obtain measurable weight loss. After conducting the experiments, the eroded specimens were

washed by using ethanol, dried with a heat gun, and placed in silica gel to avoid moisture absorption. Mass loss was calculated by using following formula.

$$\text{Erosion-Corrosion Rate} = \frac{Initial\ weight - Final\ weight}{\text{Impact Area} \times \text{Test Time}} \quad (3.3)$$

The eroded weight was measured in kg/s-m^2 (for conversion into mm/yr the conversion factor 4.04x106 was multiplied with obtained results). The experimental test matrix for multilayer painted specimens and mirror polished specimens was same. Table 3.5 shows this test matrix.

Table 3. 4 A test matrix for multilayer painted plates and mirror polished plates.

Velocity (m/s)	Particles size (microns)	Impact angle (degrees)
4	50	30
4	50	60
4	50	90
4	60	30
4	60	60
4	60	90
6	50	30
6	50	60
6	50	90
6	60	30
6	60	60
6	60	90
8	50	30
8	50	60
8	50	90
8	60	30
8	60	60
8	60	90

3.5 Quantitative and Qualitative Analysis Approaches

Degradation of specimen was studied by employing both qualitative and quantitative approaches. Quantitative approach was included mass loss analysis and erosion rate calculation while qualitative approach was comprised of multilayer paint modeling,

simple microscopic imaging and scanning electron microscopy. Figure 3.35 illustrates these approaches.

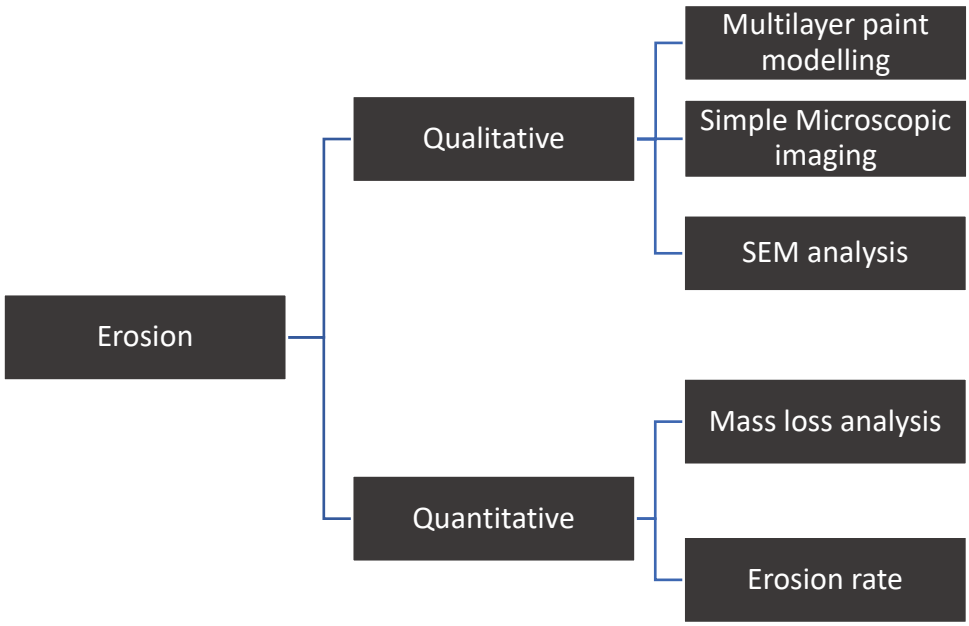

Figure 3. 35 Approaches for erosion mechanism

3.5.1 Mass Loss Analysis

It is a quantitative approach that is used for measuring the erosion rate. In this technique, erosion rate is calculated by using equation 3.3 which is mentioned above. Weight of specimen before and after testing, test time, and impact area were determined to calculate the erosion rate.

Carat balance JET503C/00 was used to measure weight of plates before and after testing. This balance was used because it can read up to 0.1 mg weight. Weight was measured in grams up to three decimal places. Figure 3.36 represents this weight balance. Stopwatch was used to measure test time, while impact area was determined by measuring the diameter of that area.

Figure 3. 36 A Carat balance JET503C/00

3.5.2 Microscopic Imaging Approach

Simple microscopic analysis and scanning electron microscopy was also used to examine mirror polished plates after testing. A digital USB 8 LEDs 500X magnifier microscope was used to observe the plates after testing. Figure 3.37 shows this magnifier microscope. Carl Zeiss AG - SUPRA 55VP scanning electron microscope was employed after testing. SEM helps in better analysis of specimen after testing as it provides clear pictures of them. It gives physical information about the erosion mechanism after testing. Concentration of each element can be found out through scanning electron microscopy. Figure 3.38 represents scanning electron microscope used after testing.

Figure 3. 37 A simple magnifier microscope

Figure 3. 38 A Scanning Electron Microscope

3.6 Summary

This chapter explains the overall methodology adopted to develop an experimental setup and find the qualitative and quantitative results. It discusses the preparation of specimen, design, and fabrication of experimental setup. Grinding, multilayer painting, and mirror polishing were considered for preparation of specimen. Following the preparation of specimen, 3D CAD model of experimental setup and then fabrication of this setup was done. This chapter also focuses on procedures adopted during testing. Different analysis approaches are also discussed in this chapter. These include both qualitative and quantitative approaches.

CHAPTER 4

RESULTS AND DISCUSSION

4.1 Introduction

This chapter discusses the conclusions based on methodology that has been explained earlier in chapter 3. The numerical and experimental results of solid particles erosion in multiphase flow condition was also compared with precedent studies of related subjects. Moreover, the working of experimental setup and measurements taken during multilayer paint modelling and mirror polished plates testing are described. The results from quantitative and qualitative analysis have been analyzed and compared to link qualitative inferences on erosion location and distribution with erosion-corrosion mechanism. The extent of erosion-corrosion in multiphase flow was determined Using qualitative and quantitative measuring techniques. The result of qualitative analysis includes multilayer paint modelling are also discussed. Therefore, quantitative results belonging to the liquid-solid flow experiment was explained. Direct impact test method is used on flat carbon steel plates. Consequently, erosion patterns on surface, microscopic imaging, and SEM/EDX analysis was performed to know the behavior of low carbon steel on different parameters and flow speeds. Results of erosion patterns on surface of MPM are described in section 2. Mass loss and Erosion rate are described in section 3 and 4. Effect of sand size, flow speed and impact angle on material removal is present in section 6 through microscopic imaging. Results obtained from SEM/EDX analysis of three different samples are explained in section 5. The general description of current chapter is given below.

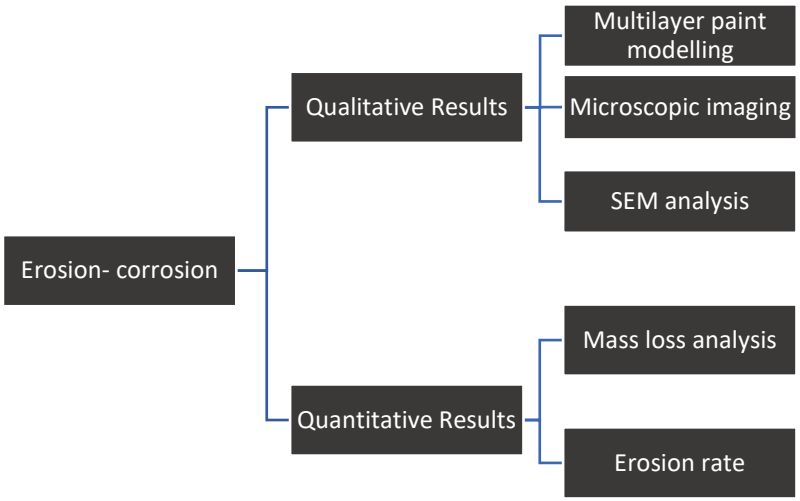

Figure 4. 1 The general overview of current chapter

4.2 Multilayer Paint Modelling MPM

The erosion behavior of multilayer paint coating, under liquid-solid flow was examined in MPM. Three layers of paint, red followed by yellow and then silver was coated on flat carbon steel plates with a well- defined thickness to extract patterns of erosion hotspots. Figures show the pattern of paint removal in a 90°, 60° and 30° impact angles and 4,6 and 8m/s flow velocity with fine sand particle. Each specimen is observed under different parameter with same time span of 30 minutes.

8m/s 6m/s 4m/s

Figure 4. 2 Paint erosion pattern for erosive solid-liquid flow with 90-degrees impact angle

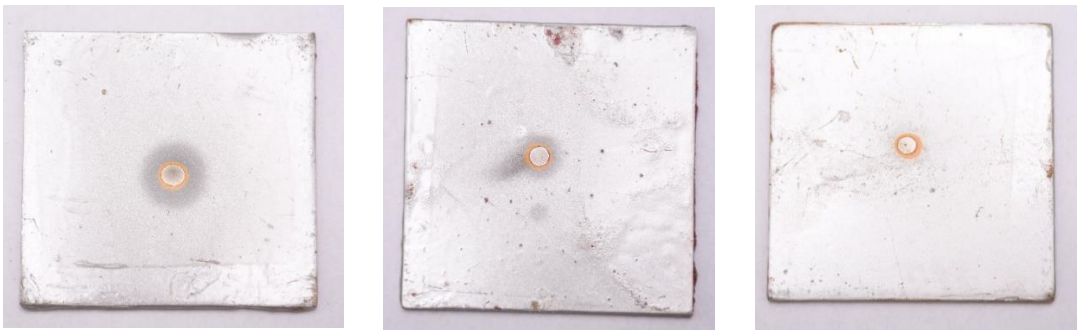

8 m/s 6 m/s 4 m/s

Figure 4. 3 Paint erosion pattern for erosive solid liquid-flow with 60-degrees impact angle

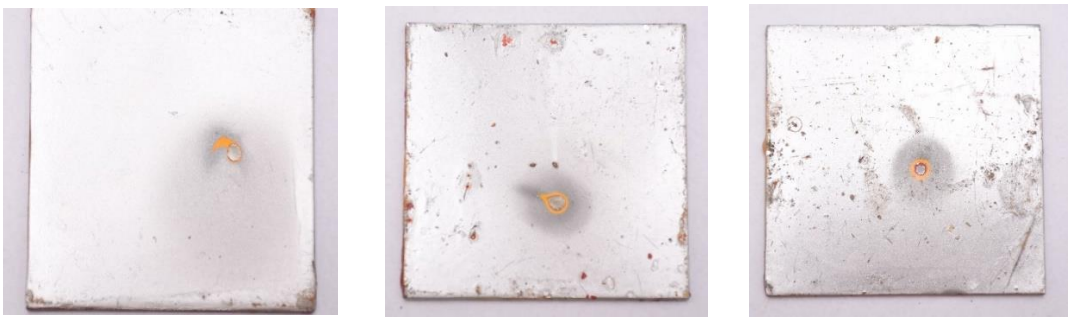

8 m/s 6 m/s 4 m/s

Figure 4. 4 Paint erosion pattern for erosive solid liquid-flow with 30-degrees impact angle

Figure 4.2 to 4.4 shows the qualitative paint erosion patterns with the location of maximum erosion on flat steel plates on liquid solid flow with impact of sand fine particles. An important factor to know the mechanism of particle wall impaction under solid liquid flow is to know the extent of particle impact in multiphase flow. Figure 4.2 shows the zone of high erosion patterns at impact angle of 90 degree at three different speeds of 8, 6 and 4 meter per second respectively. The results obtained from the current study shows that maximum erosion occurs in the range of 60-to-90-degree angles. Additional observation that are observed during the study shows that at lower angles scars are dominant and mass loss is typically less, while with increasing angle mass removal increases.

4.3 Mass loss Analysis

Mass Loss analysis was performed on flat steel plates after 30 minutes of testing multilayer painted plate and 150 minutes in case of mirror polished plates. The sand concentration was fixed but parameters like impact angles, impact speed and abrasive particle size results in different mass loss for each specimen. Mass loss was measured by carat balance normally used by jewelers.

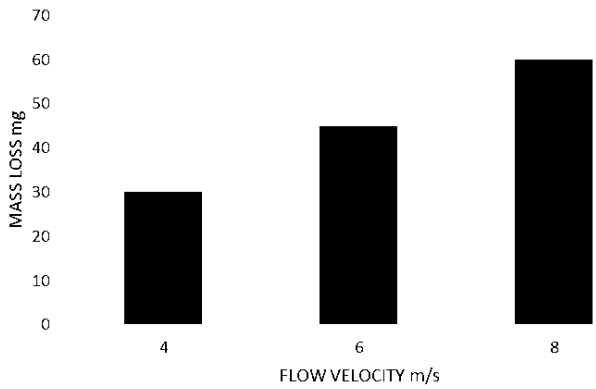

Figure 4. 5 Mass loss in 90 degrees AISI 1018 Carbon flat steel plat after exposure of slurry flow for 150 min

Table 4. 1 Mass loss rates of tested 90 degrees flat plate for Liquid-solid flow

Material	Velocity (m/s)	Particle size (µm)	Flow time (min)	Impact angle	Mass loss (mg)
1018 CS	4	50	150	90	30
1018 CS	6	50	150	90	45
1018 CS	8	50	150	90	60

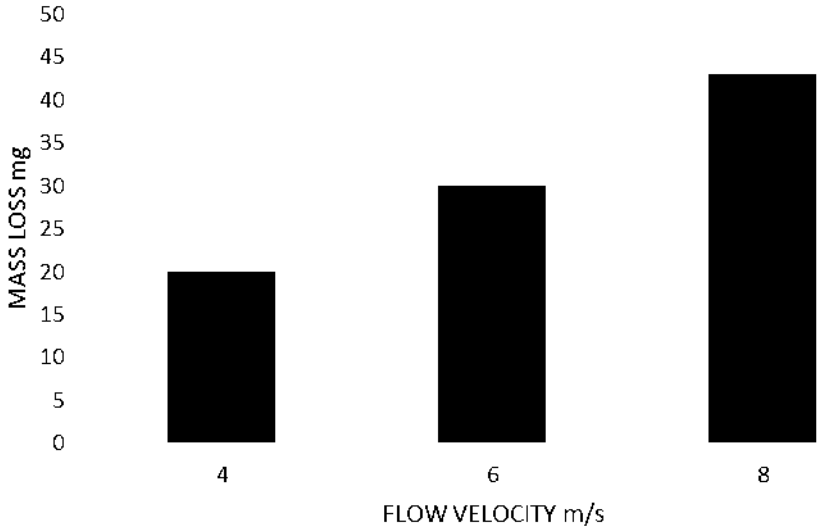

Figure 4. 6 Mass loss in 60° AISI 1018 Carbon flat steel plat after exposure of slurry flow for 150 min

Table 4. 2 Mass loss rates of tested degrees flat plate for Liquid-solid flow

Material	Velocity (m/s)	Particle size (µm)	Flow time (min)	Impact angle	Mass loss (mg)
1018 CS	4	50	150	60	20
1018 CS	6	50	150	60	30
1018 CS	8	50	150	60	43

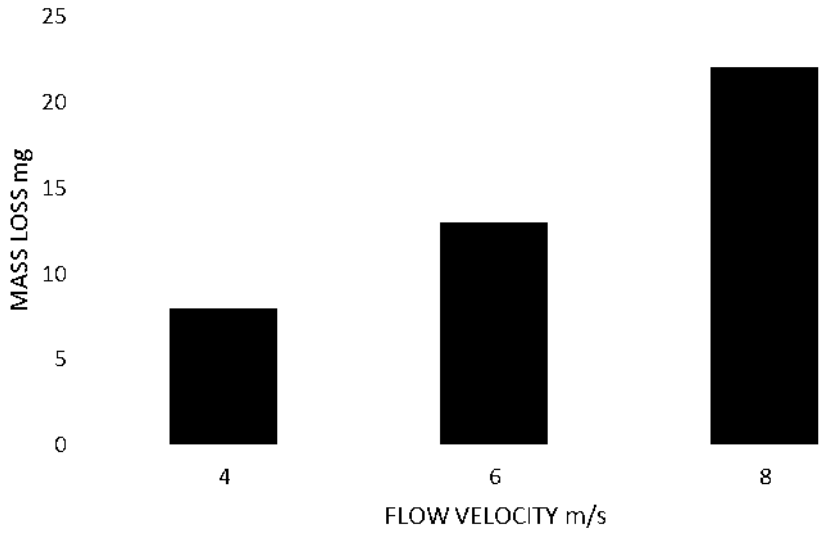

Figure 4. 7 Mass loss in 30 degrees AISI 1018 Carbon flat steel plat after exposure of slurry flow for 150 min

Table 4. 3 Mass loss rates of tested 30° flat plate for Liquid-solid flow

Material	Velocity (m/s)	Particle size (µm)	Flow time (min)	Impact angle	Mass loss (mg)
1018 CS	4	50	150	30	8
1018 CS	6	50	150	30	13
1018 CS	8	50	150	30	22

From figure 4.5 to 4.7, mass loss of specimen eroded using 50 micrometer abrasive sand particles having the angles 90, 60 and 30 degrees respectively. After observing the result

of mass loss using carrot weight it is conclude that the mass losses are greater for larger impact angles and high speeds as well.

Mass losses for smaller angles are relatively less than the mass losses that occurred at higher angles. The mass loss is directly related to abrasive particle size, therefore at smaller particle like 50 micrometer mass loss is less.

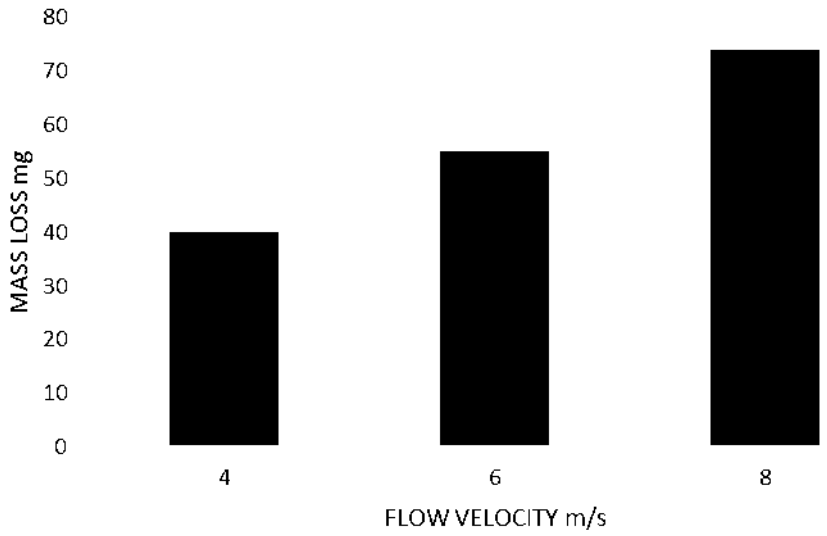

Figure 4. 8 Mass loss in 90 degrees AISI 1018 Carbon flat steel plat after exposure of slurry flow for 150 min

Table 4. 4 Mass loss rates of tested 90° flat plate for Liquid-solid flow

Material	Velocity (m/s)	Particle size (µm)	Flow time (min)	Impact angle	Mass loss (mg)
1018 CS	4	60	150	90	40
1018 CS	6	60	150	90	55
1018 CS	8	60	150	90	74

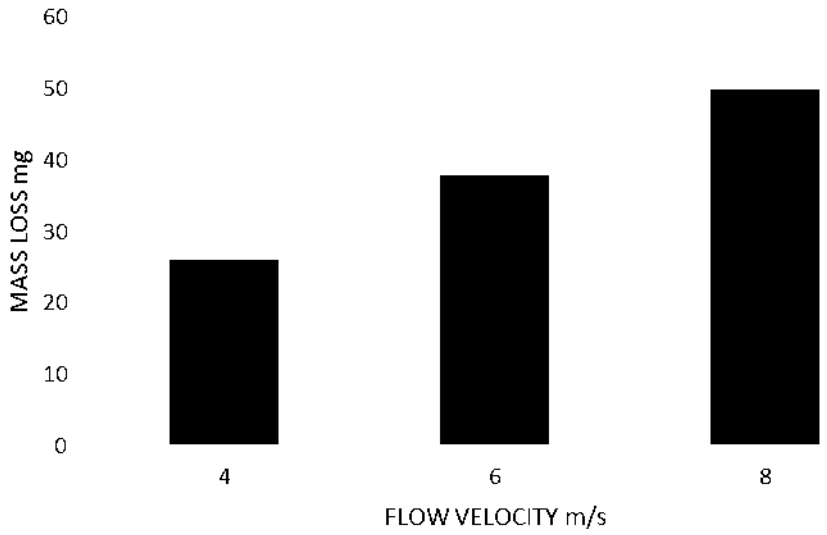

Figure 4. 9 Mass loss in 60° AISI 1018 Carbon flat steel plat after exposure of slurry flow for 150 min

Table 4. 5 Mass loss rates of tested 60° flat plate for Liquid-solid flow

Material	Velocity (m/s)	Particle size (µm)	Flow time (min)	Impact angle	Mass loss (mg)
1018 CS	4	60	150	60	26
1018 CS	6	60	150	60	38
1018 CS	8	60	150	60	49

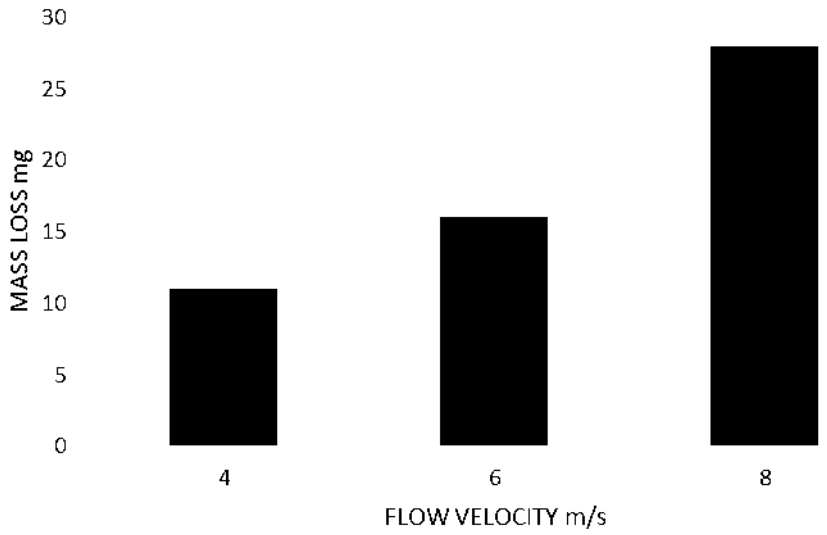

Figure 4. 10 Mass loss in 30° AISI 1018 Carbon flat steel plat after exposure of slurry flow for 150 min

Table 4. 6 Mass loss rates of tested 30° flat plate for Liquid-solid flow

Material	Velocity (m/s)	Particle size (µm)	Flow time (min)	Impact angle	Mass loss (mg)
1018 CS	4	60	150	30	11
1018 CS	6	60	150	30	16
1018 CS	8	60	150	30	28

From figure 4.8 to 4.10, mass loss of specimen eroded using 60 micrometer abrasive sand particles having the angles 90, 60 and 30 degrees respectively. After observing the result of mass loss using carrot weight it is conclude that the mass losses are greater for larger impact angles and high speeds as well. Mass losses for smaller angles are relatively less than the mass losses that occurred at higher angles. The mass loss is directly related to abrasive particle size, therefore for larger particle sizes like 60 micrometer mass losses are relatively more than 50 micrometer particle sizes.

4.4 Erosion-rate calculation

Erosion-rate or mass loss rate of our testing specimens experimented under different parameters can be calculated by using equation 3.3 which is mentioned above in chapter 3.

Erosion – Corrosion rate = (Initial Weight – Final Weight)/ (Impact area * Test Time) (4.1)

Where,

Initial Weight – Final Weight = Mass loss of eroded material

Impact Area = Area of water impacting jet on surface

Test Time = 150 min or 90000 sec

Erosion rate of all specimens having different mass losses after being tested under different parameters are shown in tables below.

Table 4. 7 Erosion rate of tested AISI carbon steel plate for 90-degree angle and 50 micrometer sand particles

Material	Impact area (m^2)	Test time (sec)	Mass loss (mg)	Erosion rate (kg/m^2s)
1018 CS	0.0036	9000	30	9.3E-7
1018 CS	0.0036	9000	45	1.39E-6
1018 CS	0.0036	9000	60	1.85E-6

Table 4. 8 Erosion rate of tested AISI carbon steel plate for 60-degree angle and 50 micrometer sand particles

Material	Impact area (m^2)	Test time (sec)	Mass loss (mg)	Erosion rate (kg/m^2s)
1018 CS	0.0036	9000	20	6.17E-7
1018 CS	0.0036	9000	30	9.3E-7
1018 CS	0.0036	9000	43	1.3E-6

Table 4. 9 Erosion rate of tested AISI carbon steel plate for 30-degree angle and 50 micrometer sand particles

Material	Impact area (m^2)	Test time (sec)	Mass loss (mg)	Erosion rate(kg/m^2s)
1018 CS	0.0036	9000	8	2.5E-7
1018 CS	0.0036	9000	13	4.0E-7
1018 CS	0.0036	9000	22	6.7E-7

Table 4. 10 Erosion rate of tested AISI carbon steel plate for 90-degree angle and 60 micrometer sand particles

Material	Impact area (m^2)	Test time (sec)	Mass loss (mg)	Erosion rate (kg/m^2s)
1018 CS	0.0036	9000	40	1.7E-6
1018 CS	0.0036	9000	55	1.7E-6
1018 CS	0.0036	9000	74	2.3E-6

Table 4. 11 Erosion rate of tested AISI carbon steel plate for 60-degree angle and 60 micrometer sand particles

Material	Impact area (m^2)	Test time (sec)	Mass loss (mg)	Erosion rate (kg/m^2s)
1018 CS	0.0036	9000	26	8.0E-7
1018 CS	0.0036	9000	38	1.2E-6
1018 CS	0.0036	9000	49	1.5E-6

Table 4. 12 Erosion rate of tested AISI carbon steel plate for 30-degree angle and 60 micrometer sand particles

Material	Impact area (m^2)	Test time (sec)	Mass loss (mg)	Erosion rate (kg/m^2s)
1018 CS	0.0036	9000	11	3.3E-7
1018 CS	0.0036	9000	16	4.9E-7
1018 CS	0.0036	9000	28	8.6E-7

After calculating the erosion rate using mass losses of different parameters, we observed that erosion rate is maximum for larger impact angle and greater speed. Erosion rate decreases with the decrease in angle and speed. By comparing the erosion rate of different sand particles sizes the one with larger particle size has greater erosion rate relatively to smaller particle sizes.

4.5 EDS (Energy dispersive x-ray spectroscopy) analysis

An SEM or EDS analysis of eroded AISI 1018 low carbon steel flat plate surface was conducted to examine the x-ray spectrum and scattering of elemental phase after the erosion-corrosion test and the color-coded dot maps plus the atomic weight percentage of each type of element in sample are shown in Figure 4.11 to Figure 4.13

The EDS mapping shows the abundance of iron atoms outside the pit on the specimen surface after testing. However, the detected level of iron atoms decreases inside the pit while growth of oxygen atoms founded inside the pit. Therefore, it can be concluded that growth in oxygen level is a symbol of pit containing iron oxide deposits increases

localized corrosion inside the pit. It is significant to highlight presence of silicon in abundance on surface.

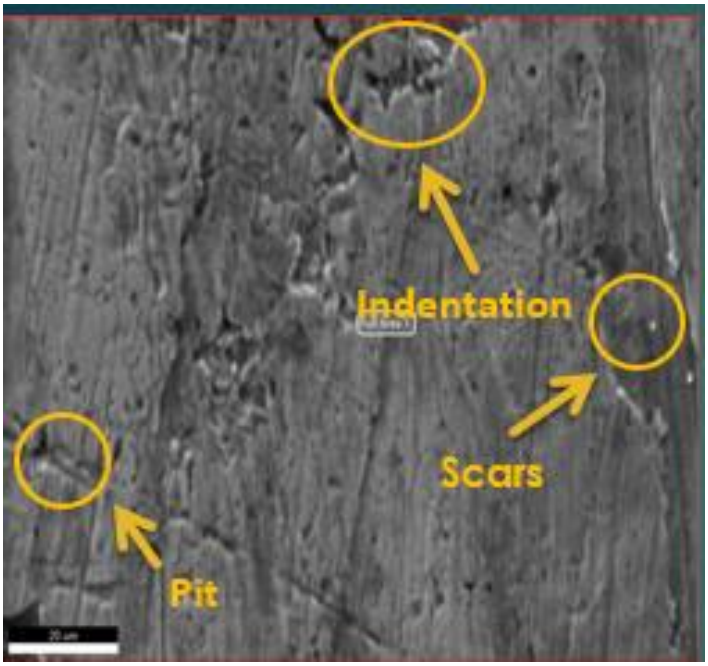

Figure 4. 11 EDS map of 90° flat mirror polished carbon steel surface after the test

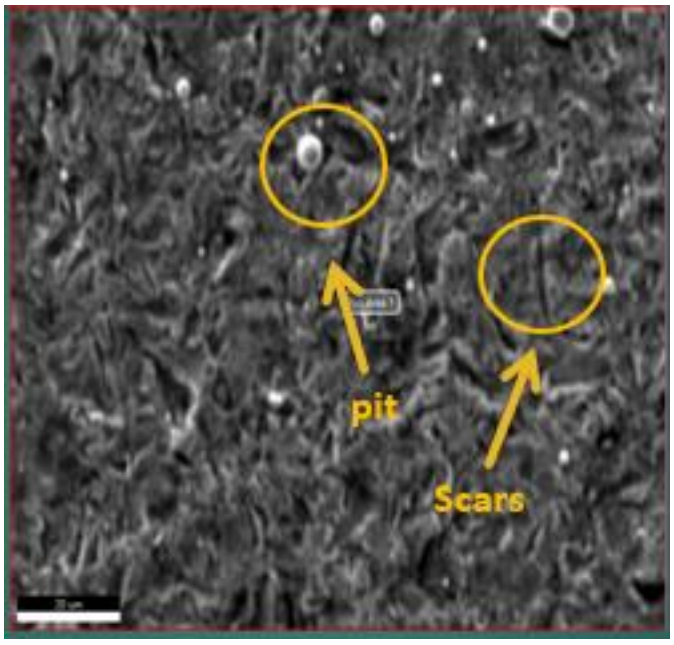

Figure 4. 12 EDS map of 60° flat mirror polished carbon steel surface after the test

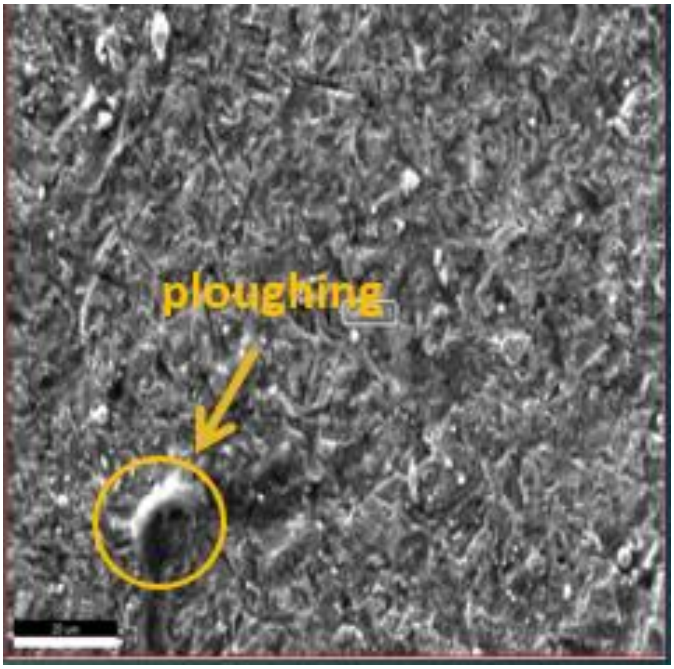

Figure 4. 13 EDS map of 30° flat mirror polished carbon steel surface after the test

The electron micrograph of the corrosion products inside and outside the pits for 90-, 60- and 30-degree impact angles is shown in the given section. The surface of the corrosion product film on pits for higher angle like 90 degree was reasonably uniform right at the center and scattered equally on the sample and elements concentration was evident proof of erosion. Similarly for 60° and 30° the erosion – corrosion patterns occurred at edges of sample as shown in Figure 4.11 to Figure 4.13

It is found that after erosion corrosion, considerable rise in weight percentage of carbon and oxygen, based on EDX spectrum analysis. Meanwhile, the weight percentage of carbon and oxygen inside and outside pit is very less. The weight percentage of iron reduces inside the pit. It is also observed carbon dioxide provokes uniform corrosion outside the pit and corrosion level is less consisting of several main elements including Fe, C, O and Si, having the weight percentage of the ranges between 73.3- 84.9, 7.2-11.2, 6.6- 9.4 and 0.9- 1.3 respectively. The spectrum shows that the particle contains feco3, fe2o3 and silica particles. A comparison of three different elemental phase distribution is shown in figure 4.14 To figure 4.16

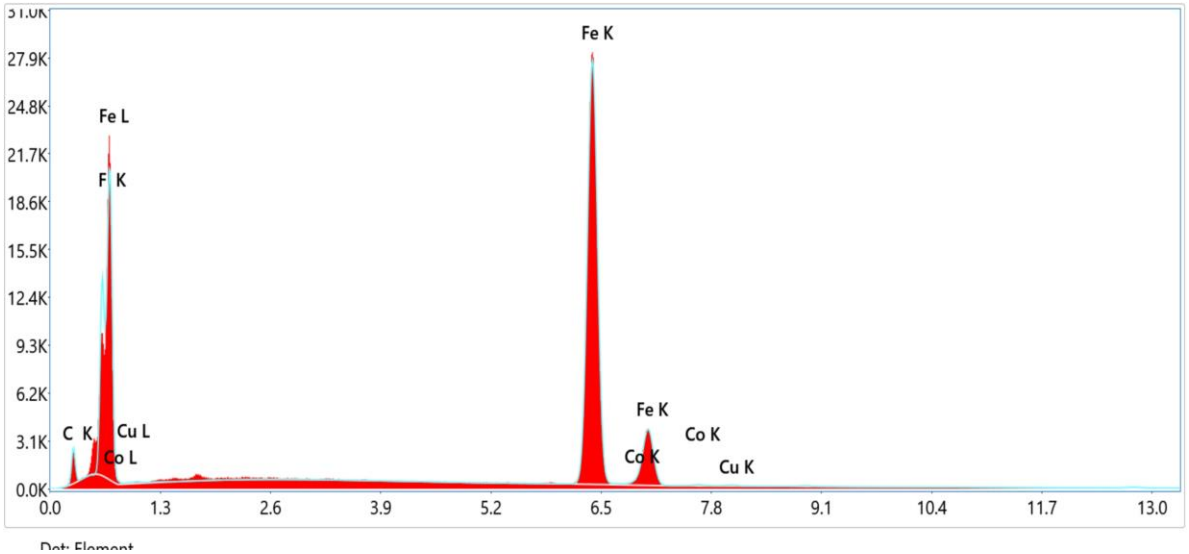

Figure 4. 14 Elemental phase spectra after the testing for 90 degree, 8meter/sec

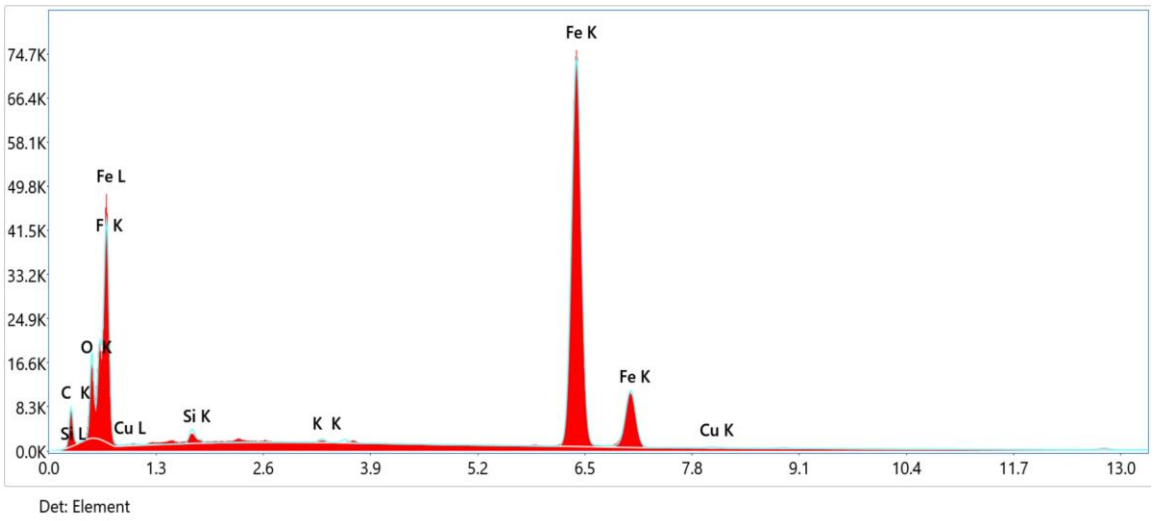

Figure 4. 15 Elemental phase spectra after the testing 1018 carbon steel for 60-degree 8meter/sec

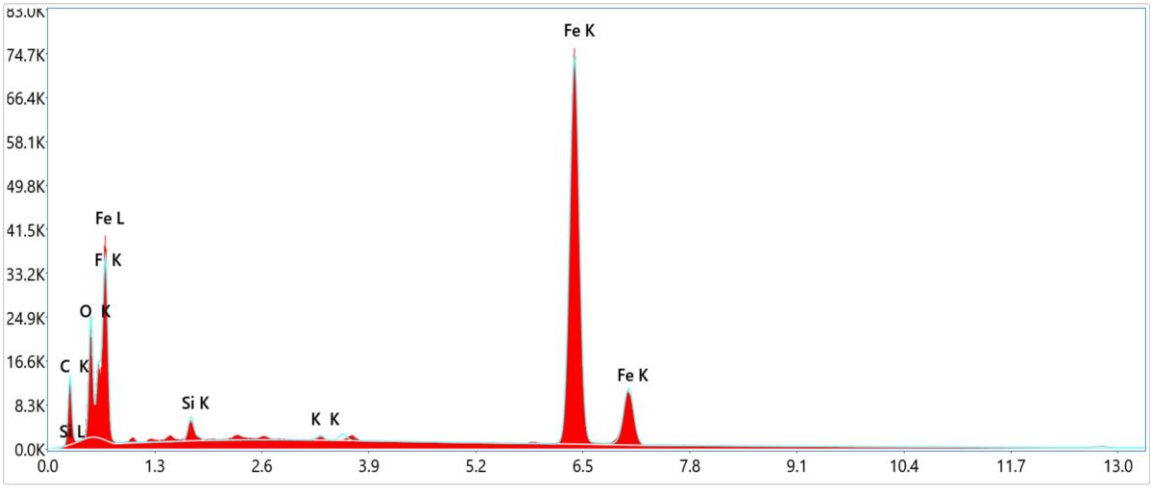

Figure 4. 16 Elemental phase spectra after the test 1018 carbon steel for 30-degree 8meter/sec

Table 4. 13 Elemental phase distribution in SEM analysis

Elements	Sample 1 90°	Sample 2 60°	Sample 3 30°
C	10	7.2	11.2
O	0	6.6	9.4
Fe	84.9	79.6	73.3
Si	0	0.9	1.3
F	4.2	5.1	4.5
K	0	0.3	0.3
Cu	0.3	0.4	0
Co	0.7	0	0

4.6 Mirror polished microscopic imaging

The erosion behavior of mirror polished plates was examined under digital industrial microscope which has resolution up to 500X, we examined the specimen on 350X resolution. From figure 4.17 to 4.19 microscopic patterns of 90-, 60- and 30-degree angles with flow speed of 4, 6 and 8 meter per second are given.

8 m/s 6 m/s 4 m/s

Figure 4. 17 Microscopic imaging analysis of eroded flat steel plate with impact angle of 90- degree

8 m/s 6 m/s 4 m/s

Figure 4. 18 Microscopic imaging analysis of eroded flat steel plate with impact angle of 60- degree

8 m/s 6 m/s 4 m/s

Figure 4. 19 Microscopic imaging analysis of eroded flat steel plate with impact angle of 30- degree

In this observation digital microscopic imaging results were presented to understand the development of erosion corrosion zones and piths on flat steel plates using different parameters like angles of 90,60 and 30 degree as shown in figure 4.17 to figure 4.19. In the first figure at 90 degrees pith depth is more because of deformation at 90 degree and

scars are less. With decrease in speed pith depth decreases. In figure 4.18 at 60-degree pith depth and scars both are prominent. In figure 4.19 at 30 degrees scars are prominent and the pith depth is very less. The reason is that at 90 degrees sand particles directly impact on the plate, so pith depths were made but in 60- and 30-degrees angle sand particles did not hit perpendicular on the flat plate, so scars were made more prominent. The number of piths in 30-degree spectrum were fewer which may be due to the less particle wall impaction. For the assessment of erosion corrosion performance in case of multiphase flow the size of perforation sites is more important.

4.7 Validation

To check whether our experimental results are valid or not, we compared our eroded sample microscopic imaging results and SEM results with the already published research. SEM micrograph of silicon sand particles on flat steel plates from already proposed research almost have same crack propagation, pit depth and thickness layer of eroded material like our results as shown in figure 4.14. Mass loss and erosion rate are approximately identical to each other and is dependent on the speed of impact and sand concentration and abrasive particle sizes.

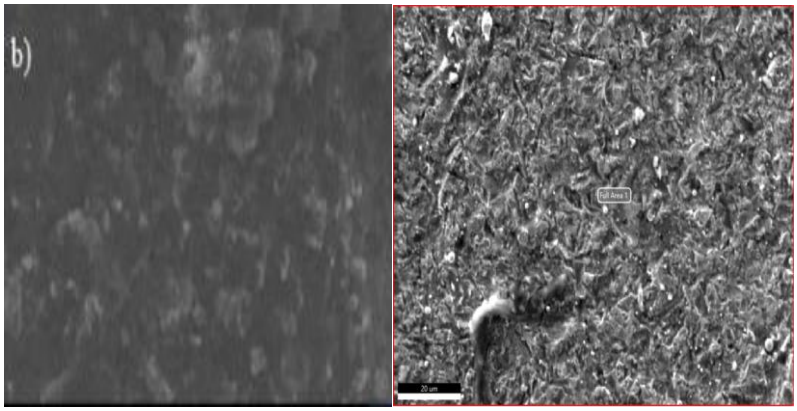

(a) D30 Previous research (b) D30 current research

Figure 4. 20 (a) Previous research r vs (b) our proposed research

4.8 Chapter summary

The result of fine sand particle erosion in multiphase flow for flat steel plate in 90 degree generated five times higher material removal rate for 50-millimeter particle sizes. Multilayer paint modelling was successfully performed for qualitative erosion distribution analysis in multiphase flow. Surface results including microscopic imaging and EDX analysis were also discussed. From the results of multiphase flow, we conclude

that that maximum particle wall impact Ness on front of the flat steel plate removes maximum material. The results of EDX analysis showed that there were traces of fine sand particles stuffed in flat plate that enhances metal corrosion. The given erosion corrosion mechanism revealed that propagation and development of pith at large angle and greater speed is high. Mass loss and Erosion rate are also calculated using equations and carrot balance.

CHAPTER 5

CONCLUSION AND FUTURE RECOMMENDATIONS

This chapter shows the total findings of the research with ending remarks. It also presents us the potential of the research along with future recommendations for further research in the field.

5.1: Conclusions

In this research, all the experimental data of erosion corrosion was gathered in solid liquid flow conditions. The current examination has increased our knowledge of fine sand particles in solid liquid flow. Erosion performance of flat AISI 1018 low carbon steel under impact angles of 90, 60 and 30 degrees and flow velocity of 8, 6 and 4m/s. The direct mass loss and erosion rates are calculated using carrot balance and erosion rate equation 4.1 MPM analysis, microscopic imaging and EDX/SEM analysis were employed to find the degradation behavior. The research aims to find erosion behavior of fine sand particles under parameters of impact angle and flow speed. The main conclusion taken from research are as follows:

1. In multiphase flow, changings in solid liquid flow velocity alters the erosion distribution and escalate particles wall interactions thus increment in the erosion rate. The experimental result shows at 90 degree and 8m/s the material degradation is more than double than 30 degree and 8m/s.
2. According to microscopic imaging, the formation of large and thick erosion corrosion pits occurs at angles around 90 degrees and maximum flow velocity. While at low angles pit depth is less and scars pattern are greater like in 30 degrees impact Ness. The different sand fines concentration has also some effect on the degradation of material.
3. It was observed that impact wear at angles of 90 and 60 degrees results in larger size erosion pits, while at 30 degrees maximum scars are present as flow is deflected at lower angles towards bottom of flat plate.

5.2: Research Contribution

Upon the completion of the above objectives, the given research is expected to give the following contributions:

i. This research shows the contribution of knowing the erosion corrosion mechanism of different parameters of angles and speed for direct impact test method. The experimental setup design, proposed methodology and research parameters in liquid solid flow conditions is closest to industrial problem of erosion corrosion.

ii. The engineers and designers of industries need to have knowledge about the multiple erosion corrosion degradation behavior in flow pipelines of oil fields. Quantification of all these parameters would be helpful to design and select material for industrial work.

iii. At present, the research on fine sand particles is very limited in solid liquid flow conditions. With the given qualitative and quantitative results of degradation of material, there can be a better prediction of introducing correction factors to save resources and assets of industry.

5.3: Future Works Recommendations

i. Despite this research provides good qualitative and quantitative comparison of solid liquid flow, however for better understanding of the erosion corrosion mechanism further studies are important by incorporating thickness of pit and using sand concentration factor.

ii. The further research is recommended on the same parameters of impact angles and speed by using CFD analysis and by applying Vickers hardness on specimens. By comparing the results of CFD simulation with microscopic imaging and SEM analysis, one can have better understanding on complete erosion corrosion behavior.

References

1. Mansouri, A., *A combined CFD-experimental method for developing an erosion equation for both gas-sand and liquid-sand flows*. 2016: The University of Tulsa.
2. Jha, A., et al., *Effect of impinging angle and rotating speed on erosion behavior of aluminum.* Transactions of Nonferrous Metals Society of China, 2011. **21**(1): p. 32-38.
3. Steward, N. and A. Spearing, *Combating pipeline wear-an advancing technology.* Journal of the Southern African Institute of Mining and Metallurgy, 1992. **92**(6): p. 149-157.
4. Parsi, M., et al., *A comprehensive review of solid particle erosion modeling for oil and gas wells and pipelines applications*, in *Journal of Natural Gas Science and Engineering*. 2014. p. 850-873.
5. Forder, A., M. Thew, and D. Harrison, *A numerical investigation of solid particle erosion experienced within oilfield control valves.* Wear, 1998. **216**(2): p. 184-193.
6. Appah, D., *New gravel-pack technique reduces sand production in Niger delta wells.* Oil & Gas Journal, 2001. **99**(27): p. 44-44.
7. Lin, H., S. Wu, and C. Yeh, *A comparison of slurry erosion characteristics of TiNi shape memory alloys and SUS304 stainless steel.* Wear, 2001. **249**(7): p. 557-565.
8. Bitter, J., *A study of erosion phenomena part I.* wear, 1963. **6**(1): p. 5-21.
9. Bitter, J., *A study of erosion phenomena: Part II.* Wear, 1963. **6**(3): p. 169-190.
10. Clark, H.M. and K.K. Wong, *Impact angle, particle energy and mass loss in erosion by dilute slurries.* Wear, 1995. **186**: p. 454-464.
11. Humphrey, J., *Fundamentals of fluid motion in erosion by solid particle impact.* International journal of heat and fluid flow, 1990. **11**(3): p. 170-195.
12. Clark, H.M., *The influence of the flow field in slurry erosion.* Wear, 1992. **152**(2): p. 223-240.
13. Clark, H.M. and R.B. Hartwich, *A re-examination of the 'particle size effect' in slurry erosion.* Wear, 2001. **248**(1-2): p. 147-161.
14. Zu, J., I. Hutchings, and G. Burstein, *Design of a slurry erosion test rig.* Wear, 1990. **140**(2): p. 331-344.

15. Levy, A. and G. Hickey, *Liquid-solid particle slurry erosion of steels.* Wear, 1987. **117**(2): p. 129-146.
16. Levy, A.V., J. Yan, and V.D. Arora, *Sand-water slurry erosion of carburized AISI 8620 steel.* Wear, 1985. **101**(2): p. 117-126.
17. Mazumder, Q.H., et al., *Development and validation of a mechanistic model to predict solid particle erosion in multiphase flow.* Wear, 2005. **259**(1-6): p. 203-207.
18. Desale, G.R., B.K. Gandhi, and S. Jain, *Slurry erosion of ductile materials under normal impact condition.* Wear, 2008. **264**(3-4): p. 322-330.
19. Desale, G.R., B.K. Gandhi, and S. Jain, *Effect of erodent properties on erosion wear of ductile type materials.* Wear, 2006. **261**(7-8): p. 914-921.
20. Al-Bukhaiti, M., et al., *Effect of impingement angle on slurry erosion behaviour and mechanisms of 1017 steel and high-chromium white cast iron.* Wear, 2007. **262**(9-10): p. 1187-1198.
21. Burstein, G. and K. Sasaki, *Effect of impact angle on the slurry erosion–corrosion of 304L stainless steel.* Wear, 2000. **240**(1-2): p. 80-94.
22. Gandhi, B.K., S. Singh, and V. Seshadri, *Study of the parametric dependence of erosion wear for the parallel flow of solid–liquid mixtures.* Tribology international, 1999. **32**(5): p. 275-282.
23. Levy, A.V. and P. Yau, *Erosion of steels in liquid slurries.* Wear, 1984. **98**: p. 163-182.
24. Wood, R., et al., *Comparison of predicted and experimental erosion estimates in slurry ducts.* Wear, 2004. **256**(9-10): p. 937-947.
25. Brennen, C.E. and C.E. Brennen, *Fundamentals of multiphase flow.* 2005.
26. Naz, M.Y., et al., *Erodent Impact Angle and Velocity Effects on Surface Morphology of Mild Steel.* Procedia engineering, 2016. **148**: p. 896-901.
27. Parsi, M., et al., *A comprehensive review of solid particle erosion modeling for oil and gas wells and pipelines applications.* Journal of Natural Gas Science and Engineering, 2014. **21**: p. 850-873.
28. Elemuren, R., et al., *Slurry erosion-corrosion of 90 AISI 1018 steel elbow in saturated potash brine containing abrasive silica particles.* Wear, 2018. **410**: p. 149-155.
29. Finnie, I., *Some observations on the erosion of ductile metals.* wear, 1972. **19**(1): p. 81-90.

30. Levy, A.V., *The platelet mechanism of erosion of ductile metals.* Wear, 1986. **108**(1): p. 1-21.
31. Hutchings, I. and R. Winter, *Particle erosion of ductile metals: a mechanism of material removal.* Wear, 1974. **27**(1): p. 121-128.
32. Tilly, G., *A two stage mechanism of ductile erosion.* Wear, 1973. **23**(1): p. 87-96.
33. Levy, A.V. and P. Chik, *The effects of erodent composition and shape on the erosion of steel.* Wear, 1983. **89**(2): p. 151-162.
34. Meng, H. and K. Ludema, *Wear models and predictive equations: their form and content.* Wear, 1995. **181**: p. 443-457.
35. Xie, Y., H.M. Clark, and H. Hawthorne, *Modelling slurry particle dynamics in the Coriolis erosion tester.* Wear, 1999. **225**: p. 405-416.
36. Javaheri, V., D. Porter, and V.-T. Kuokkala, *Slurry erosion of steel–Review of tests, mechanisms and materials.* Wear, 2018. **408**: p. 248-273.
37. Laitone, J., *Aerodynamic effects in the erosion process.* Wear, 1979. **56**(1): p. 239-246.
38. Oka, Y.I., K. Okamura, and T. Yoshida, *Practical estimation of erosion damage caused by solid particle impact: Part 1: Effects of impact parameters on a predictive equation.* Wear, 2005. **259**(1-6): p. 95-101.
39. Hutchings, I.M., *Ductile-brittle transitions and wear maps for the erosion and abrasion of brittle materials.* Journal of Physics D: Applied Physics, 1992. **25**(1A): p. A212.
40. Arabnejad, H., et al., *The effect of erodent particle hardness on the erosion of stainless steel.* Wear, 2015. **332**: p. 1098-1103.
41. Sarlin, E., et al., *High-temperature slurry erosion of vinylester matrix composites–The effect of test parameters.* Wear, 2015. **328**: p. 488-497.
42. Nguyen, V., et al., *Effect of air-borne particle–particle interaction on materials erosion.* Wear, 2015. **322**: p. 17-31.
43. Dai, L., et al., *Analysis and comparison of long-distance pipeline failures.* Journal of Petroleum Engineering, 2017. **2017**.
44. Alam, T. and Z.N. Farhat, *Slurry erosion surface damage under normal impact for pipeline steels.* Engineering Failure Analysis, 2018. **90**: p. 116-128.
45. Alamu, M. and B. Azzopardi, *Simultaneous investigation of entrained liquid fraction, liquid film thickness and pressure drop in vertical annular flow.* Journal of energy resources technology, 2011. **133**(2).

46. Lindgren, M. and J. Perolainen, *Slurry pot investigation of the influence of erodant characteristics on the erosion resistance of titanium.* Wear, 2014. **321**: p. 64-69.
47. Tuzson, J., J. Lee, and K. Scheibe-Powell, *Slurry erosion tests with centrifugal erosion tester.* American Society of Mechanical Engineers, 1984: p. 84-87.
48. Kesana, N.R., *Erosion in multiphase pseudo slug flow with emphasis on sand sampling and pseudo slug characteristics*. 2013: The University of Tulsa.
49. Vieira, R.E., *Sand erosion model improvement for elbows in gas production, multiphase annular and low-liquid flow*. 2014: The University of Tulsa.
50. Shirazi, S., et al., *A procedure to predict solid particle erosion in elbows and tees.* 1995.
51. McLaury, B.S. and S.A. Shirazi, *An alternate method to API RP 14E for predicting solids erosion in multiphase flow.* J. Energy Resour. Technol., 2000. **122**(3): p. 115-122.
52. Salama, M. and E. Venkatesh. *Evaluation of API RP 14E erosional velocity limitations for offshore gas wells*. in *Offshore technology conference*. 1983. OnePetro.
53. Svendeman, S., K. Arnold, and S.P. Facil, *'Criteria for Sizing Multi-phase Flow Lines for Erosive/Corrosive Services.* SPE Prod. Facil, 1994. **9**: p. 74-80.
54. Salama, M.M. *An alternative to API 14E erosional velocity limits for sand laden fluids*. in *Offshore technology conference*. 1998. OnePetro.
55. McLaury, B.S., et al. *Effect of upstream pipe orientation on erosion/corrosion in bends for annular flow*. in *CORROSION 2006*. 2006. OnePetro.
56. Ahlert, K.R., *Effects of particle impingement angle and surface wetting on solid particle erosion of AISI 1018 steel*. 1994, BUniversity of Tulsa.